2014-03

Imaging gallium nitride high electron mobility transistors to identify point defects

Wessel, Ashley M.

Monterey, California: Naval Postgraduate School

NAVAL POSTGRADUATE SCHOOL

MONTEREY, CALIFORNIA

THESIS

IMAGING GALLIUM NITRIDE HIGH ELECTRON MOBILITY TRANSISTORS TO IDENTIFY POINT DEFECTS

by

Ashley M. Wessel

March 2014

Thesis Advisor: Todd R. Weatherford
Second Reader: Matthew A. Porter

Approved for public release; distribution is unlimited

THIS PAGE INTENTIONALLY LEFT BLANK

REPORT DOCUMENTATION PAGE

Form Approved OMB No. 0704-0188

1. AGENCY USE ONLY *(Leave blank)*	**2. REPORT DATE** March 2014	**3. REPORT TYPE AND DATES COVERED** Master's Thesis

4. TITLE AND SUBTITLE
IMAGING GALLIUM NITRIDE HIGH ELECTRON MOBILITY TRANSISTORS TO IDENTIFY POINT DEFECTS

5. FUNDING NUMBERS

6. AUTHOR(S) Ashley M. Wessel

7. PERFORMING ORGANIZATION NAME(S) AND ADDRESS(ES)
Naval Postgraduate School
Monterey, CA 93943-5000

8. PERFORMING ORGANIZATION REPORT NUMBER

9. SPONSORING /MONITORING AGENCY NAME(S) AND ADDRESS(ES)
N/A

10. SPONSORING/MONITORING AGENCY REPORT NUMBER

11. SUPPLEMENTARY NOTES The views expressed in this thesis are those of the author and do not reflect the official policy or position of the Department of Defense or the U.S. Government. IRB protocol number ____N/A____.

12a. DISTRIBUTION / AVAILABILITY STATEMENT
Approved for public release; distribution is unlimited

12b. DISTRIBUTION CODE
A

13. ABSTRACT (maximum 200 words)

The purpose of this thesis is to streamline the sample preparation procedure to maximize the yield of successful samples to be analyzed chemically in an energy dispersive spectrometry detector. The secondary objective of this work is to identify the specific chemical elements needed to ascertain trends in stressing nickel/gold and platinum/gold gated high electron mobility transistors (HEMT). We analyze unstressed devices near the hetero-epitaxial layers to ascertain any inconsistencies due to processing defects. Results show it is possible to identify areas of electrical stress-induced diffusion and point defect creation. Identification of these trends will assist in the improvement of gallium nitride HEMT fabrication processes leading to the development of more reliable devices.

14. SUBJECT TERMS Electron microscopy, Gallium Nitride (GaN), high electron mobility transistor (HEMT), , electron dispersive spectrometry (EDS), focused ion beam (FIB), scanning electron microscope (SEM), transmission electron microscope (TEM), scanning transmission electron microscope (STEM), sample preparation

15. NUMBER OF PAGES
103

16. PRICE CODE

17. SECURITY CLASSIFICATION OF REPORT	**18. SECURITY CLASSIFICATION OF THIS PAGE**	**19. SECURITY CLASSIFICATION OF ABSTRACT**	**20. LIMITATION OF ABSTRACT**
Unclassified	Unclassified	Unclassified	UU

NSN 7540-01-280-5500

Standard Form 298 (Rev. 2-89)
Prescribed by ANSI Std. 239-18

THIS PAGE INTENTIONALLY LEFT BLANK

Approved for public release; distribution is unlimited

IMAGING GALLIUM NITRIDE HIGH ELECTRON MOBILITY TRANSISTORS TO IDENTIFY POINT DEFECTS

Ashley M. Wessel
Lieutenant, United States Navy
B.S.E.E., United States Naval Academy

Submitted in partial fulfillment of the
requirements for the degree of

MASTER OF SCIENCE IN ELECTRICAL ENGINEERING

from the

NAVAL POSTGRADUATE SCHOOL
March 2014

Author: Ashley M. Wessel

Approved by: Todd R. Weatherford
Thesis Advisor

Matthew A. Porter
Second Reader

R. Clark Robertson
Chair, Department of Electrical Computer Engineering

THIS PAGE INTENTIONALLY LEFT BLANK

ABSTRACT

The purpose of this thesis is to streamline the sample preparation procedure to maximize the yield of successful samples to be analyzed chemically in an energy dispersive spectrometry detector. The secondary objective of this work is to identify the specific chemical elements needed to ascertain trends in stressing nickel/gold and platinum/gold gated high electron mobility transistors (HEMT). We analyze unstressed devices near the hetero-epitaxial layers to ascertain any inconsistencies due to processing defects. Results show it is possible to identify areas of electrical stress-induced diffusion and point defect creation. Identification of these trends will assist in the improvement of gallium nitride HEMT fabrication processes leading to the development of more reliable devices.

THIS PAGE INTENTIONALLY LEFT BLANK

TABLE OF CONTENTS

LIST OF FIGURES

LIST OF TABLES

THIS PAGE INTENTIONALLY LEFT BLANK

LIST OF ACRONYMS AND ABBREVIATIONS

2DEG	Two-dimensional gas
Al	Aluminum
Au	Gold
(Al, Ga)N	Aluminum gallium nitride
AlO_x	Aluminum oxide
CCD	Charged coupled device
CTE	Coefficient of thermal expansion
DoD	Department of Defense
DTRA	Defense Threat Reduction Agency
E-beam	Electronic beam
EDS	Energy-dispersive x-ray spectroscopy
Epi	Hetero-epitaxial
FET	Field effect transistor
FIB	Focused ion beam
GaN	Gallium nitride
HAADF	High-angle annular dark-field
HEMT	High energy mobility transistor
I-beam	Ion beam
IC	Integrated circuit
LBNL	Lawrence Berkeley National Lab
N	Nitrogen
Ni	Nickel
NRL	Naval Research Laboratory
O	Oxygen
Pt	Platinum
Si	Silicon
Si_3N_4	Silicon nitride

THIS PAGE INTENTIONALLY LEFT BLANK

EXECUTIVE SUMMARY

In this thesis we used cutting edge electron microscopy tools at Lawrence Berkeley National Lab to analyze the gate edge of both unstressed and electrically stressed gallium nitride (GaN) high electron mobility transistors (HEMTs) provided by the Naval Research Laboratory. We performed careful qualification chemical analysis using the electron dispersive spectrometry (EDS) detector to identify trends in chemical anomalies and defects within the HEMT to improve the overall reliability of the device in future processing.

We selected our sample set as shown in Table 1. We were given both nickel/gold (Au) and platinum (Pt)/Au gated HEMTs. We chose three devices of each gate type in order to have a progression of trends throughout various degradation levels of the device, and one sample of the epitaxial substrate. The seven devices listed in Table 1 created our sample set and are the foundation for the samples created. Multiple fresh or unstressed samples were found on the same integrated circuit (IC) for each gate type and the cleanest device was chosen to be our candidate for sample preparation. All devices from the sample set in Table 1 used the same sample preparation procedure.

We were able to develop, refine and optimize a new sample preparation process to meet high resolution TEM images, multiple machine transfers, and multiple ion beam exposures. We were also able to successfully identify the elements present along the gate edge of the devices and identify processing and electrical stressing trends.

The sample preparation procedure began by using the Oxford Instruments OmniProbe manipulator to lift out each sample in the focused ion beam (FIB). The sample was welded to a copper sample holder. The first thinning cut into the sample began at 1000ρA at approximately 2μm thick down to 300ρA at 200–400nm thick. The FIB thinning had reached its threshold with each sample. Another machine using a lower voltage was required in order to minimize potential preparation induced dislocations.

Table 1. Complete sample set of devices used for chemical analysis.

Pt		Stressed Levels	Stressed ID Number	FIB	TITAN
Fresh	NRL-10	NA	NA	Y	Y
Degraded	NRL-13	95V	R3GD15GF2DF2	Y	Y
Failed	NRL-12	135V	R3GD15GF2DF4	Y	Y
Ni					
Fresh	NRL-Ni-1	NA	NA	Y	Y
Degraded	NRL-Ni-3	130V	R3GD15GF2DF3	Y	Y
Failed	NRL-Ni-4	125V	R3GD15GF2DF4	Y	Y
Epi layer	NRL-Epi-1	NA	NA	Y	Y

The nano-scale ion mill (NanoMill) was used to thin the devices down to 100nm. The EDS detector required the sample to be less than 200nm [1]. The NanoMill milled the sample with a beam current of 100ρA. The milling rate was determined under our control parameters to be 1nm/min. The ion mill was focused on the active region of the sample shown in Figure 1 to maintain the structural integrity of the sample by only thinning the top region where EDS analysis would take place.

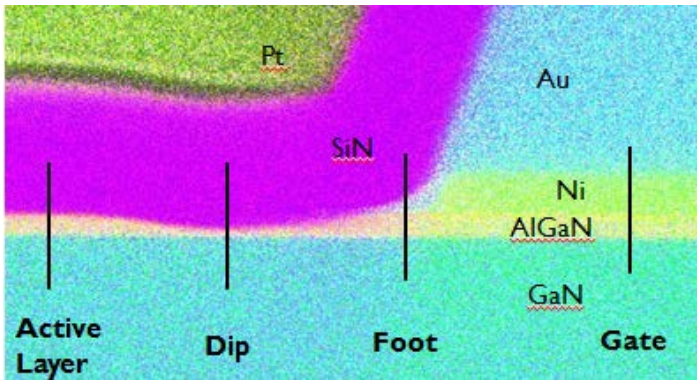

Figure 1. Ni/Au gate edge with four line scan areas labeled.

Finally the samples were imaged using a transmission electron microscope (TEM) along with the EDS detector. All seven samples were successfully imaged along the gate edge due to electroluminescence information received from the stressed devices. The Bruker© EDS software was used in conjunction with the TEM to analyze the same four line scan areas across the gate edge of all samples shown in Figure 1. The line scan data

provided the necessary information to identify specific elements present across the edge of the gate. From the seven samples analyzed, 26 line scans were compared to identify trends. The line scans were individually analyzed and compared to ascertain trends. One trend identified was the gate metal diffusion when the device was stressed, as seen in Figure 2.

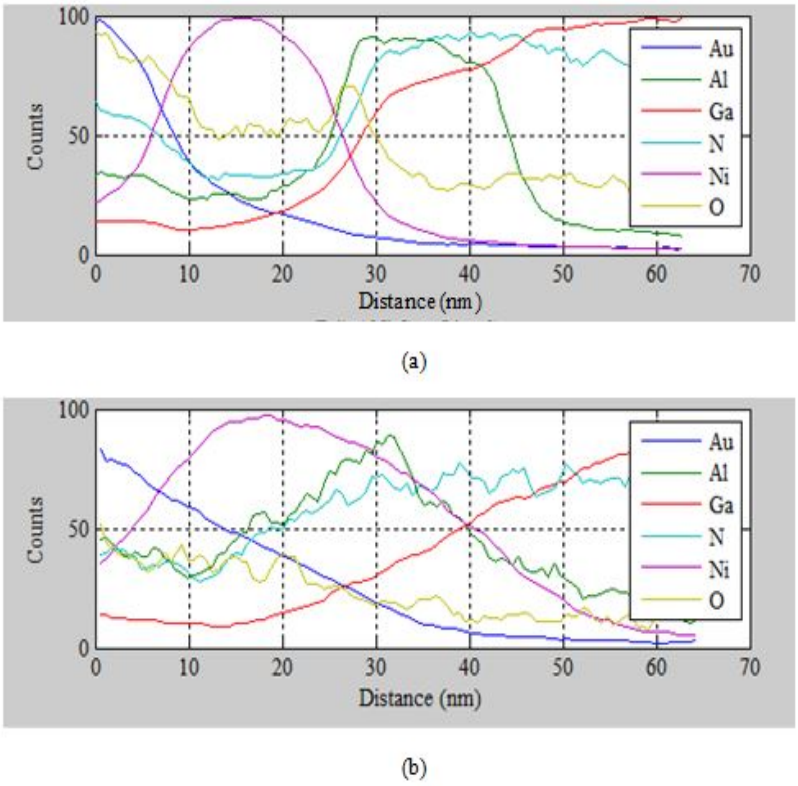

Figure 2. Frsh (a) and failed (b) Ni gate line scan data sets in distance versus detector percentage counts. The graphs depict a change in the location of Ni in the same region underneath the gate.

Based on the line scan results, we concluded there is a dominant melting defect creating an amorphous area composed of both gate metals at the gate edge and the Pt device exhibited a more noticeable melting defect in all three samples compared to the nickel samples. In all six device samples, the 2nm protective GaN cap layer was not present but was present in the preprocessed epitaxial layer sample. We also did not notice any change in the chemical composition of either the Pt or Ni samples at 100nm away

from the gate edge. We did notice a presence of oxygen in the thin aluminum gallium nitride ((Al, Ga)N) layer likely forming some amount of aluminum oxide. Finally, we noticed the gate regions in both metal gate types experienced metal diffusion into the (Al, Ga)N layer and stopping at the GaN layer, as shown in Figure 2 for the Ni device.

ACKNOWLEDGMENTS

A truly special thanks goes to Petra Specht for her willingness to impart her expertise with sample preparation, data analysis, Lawrence Berkeley National Lab (LBNL) facilities, presentation and thesis guidance, and, most importantly, her immense knowledge. This thesis would not exist without the help of her guidance throughout. The staff at LBNL was particularly helpful in furthering my knowledge on how to use the microscopes. They always made me feel welcome as well as made themselves available to answer any questions that I had through the process.

I would like to thank Dr. Weatherford for making the arrangements necessary to allow me hands-on experience in working with Dr. Specht. Working at the Lawrence Berkeley National Lab was an incredible experience that will not be forgotten. I also appreciated his guidance in honing my thesis process as well as presentation preparation.

Special thanks goes to Matthew Porter for his patience in explaining difficult topics and for organizing an independent study time on quantum mechanics as well as general help with the writing process of this thesis.

My thanks also go to my family for the sacrifices made to ensure that I could travel and spend multiple days and nights up at LBNL. I would not have been able to travel without their willingness to change their schedule to accommodate mine. Thank you also for being so understanding when my weekends were occupied with research. I could not have finished without your continued and unwavering support.

THIS PAGE INTENTIONALLY LEFT BLANK

I. INTRODUCTION

As higher frequency bands become increasingly used for radar and high bandwidth communication systems, the need for solid state power devices that can operate at high temperature and power levels increases. In the power device operating regime, reliability additionally becomes a major concern. Gallium nitride (GaN) is a group III-V semiconductor that exhibits better performance than silicon (Si) in breakdown voltage, thermal conductivity and electron mobility. These performance factors are the main reasons why GaN is replacing Si in many high-powered and high frequency applications [1], [2].

Though GaN shows promise, it is extremely expensive to manufacture as a stand-alone material. In contrast, Si is relatively inexpensive. Si wafers can be grown to the industry standard of 450 mm in diameter [3]. Bulk GaN wafers can only commercially be grown up to diameters of 50 mm [4]. This growth discrepancy means GaN substrate devices cannot be a viable option based solely on the number of devices produced on each wafer per processing run. Recent developments have enabled the growth of GaN atop Si substrates of 200mm in diameter. The growth of GaN hetero-epitaxial layers grown instead on a Si substrate capitalizes on the two main strengths of Si: cost and substrate size.

Growing semiconductors epitaxially does present limitations. Lattice mismatch between the Si and GaN induces strain in epitaxial GaN films, leading to the formation of dislocations and point defect complexes [5]. Transition layers can be introduced before the GaN layer to help with relaxation and stressing of the mismatched layers. The majority of previous research has been focused upon the study of defects arising in this location within the epitaxial layer.

A. RESEARCH OBJECTIVE

Evaluation of GaN HEMT reliability and the underlying defects has not been intensively investigated. The work in this thesis focuses on two main objectives. First, we streamline a transmission electron microscopy (TEM) sample preparation process

creating a higher yield of samples to be analyzed. Second, we identify the point defects along the source side of the gate edge of the high electron mobility transistor (HEMT) using chemical analysis through backscatter x-ray energy dispersive spectroscopy (EDS). We compare a sample set of unstressed and electrically stressed platinum (Pt) and nickel (Ni) gated HEMTs. Next, analysis of these comparisons are used to reveal chemical trends in point defects along the gate edge of the HEMTs and can lead to a more reliable HEMT in the future.

B. RELEVANCE TO THE DEPARTMENT OF DEFENSE

Shipboard and radar communication systems are mostly Si and vacuum tube based, due to either low cost or high power and reliability requirements. However, there is a growing need to replace existing infrastructure in applications requiring simultaneous high power density and high efficiency. For example, drones require radio frequency radar systems that are compact and highly efficient. GaN technology has shown great promise for these applications.

Past studies have shown GaN device reliability to be intrinsically greater than that of Si transistors. This reliability extends over regions of operation that have traditionally caused problems for Si devices, such as high temperature or high radiation environments [6], [7]. The interest of the Department of Defense (DOD) in high radiation environments lends itself perfectly to GaN technologies. Though the promise of GaN is enticing, the understanding of the underlying physics of GaN reliability, specifically in HEMT structures, remains incomplete. Further study is needed before GaN devices can be safely implemented at MILSPEC standards in DOD systems.

The Defense Threat Reduction Agency (DTRA) is currently investigating radiation induced defects within these GaN devices. This thesis is a small portion of this larger project, but still adds a significant contribution to the overarching research efforts.

C. RELATED WORK

In 2001, researchers at the Naval Postgraduate School (NPS) began studying GaN semiconductors. The published work on GaN focused on two-dimensional modeling and

the piezoelectric effect [8], [9], [10], [11]. In 2006 the first thesis from NPS [12] looked at imaging GaN using a scanning electron microscope (SEM) as well as linking the intensity of luminescence to carrier diffusion lengths of the material.

NPS currently has a SEM equipped with a focused ion beam (FIB). In 2013, D. Cary in [13] took advantage of both machines in his thesis to image GaN power transistors. NPS is scheduled to receive a scanning transmission electron microscope (STEM) with an energy-dispersive spectroscopy (EDS) detector capable of light element detection with use of associated Bruker© analysis software in April 2014. Previous work from NPS in both the electrical and applied physics departments directly supports the completion of this research.

D. THESIS ORGANIZATION

Relevant background information, starting with the building blocks of the GaN power HEMT as well as the epitaxial growth of GaN on a Si substrate is contained in Chapter II. We lay the foundation for our experiments in Chapter III by discussing sample preparation of the devices that include the use of the focused ion beam (FIB), nano-scale ion mill (NanoMill) and the scanning transmission electron microscope (STEM) with energy dispersive spectrometry (EDS) detector. Experimental procedures and analysis of results are presented in Chapter IV. Conclusions are drawn and future work proposed in in Chapter V.

THIS PAGE INTENTIONALLY LEFT BLANK

II. BACKGROUND

Si has had a long history as the primary material used for the fabrication of solid state electronics over the past 50 years. However, with the increase in need for devices that can operate at higher frequency and power levels, other semiconductor materials have been developed. Group III-V semiconductors like GaN give us superior performance in comparison with Si. Specifically, the "wide bandgap" III-V semiconductors have a large critical breakdown electric field value, as seen in Table 1, enabling the fabrication of devices with simultaneously low breakdown voltages and resistive heating losses.

Table 1. Material properties of microwave semiconductors (from [14]).

Material	Mobility, μ, $cm^2/V.s$	Dielectric Constant, ε	Bandgap, Eg, eV	Break down field, Eb 10^6V/cm
Si	1300	11.9	1.12	0.3
GaAs	5000	12.5	1.42	0.4
4H-SiC	260	10	3.2	3.5
GaN	1500	9.5	3.4	2

This chapter discusses the necessary theory behind the experiments of this thesis by addressing the fundamentals of the GaN power HEMT including how the device works as well as how a generic HEMT is fabricated. Section B looks specifically at the Naval Research Laboratory (NRL) GaN HEMTs used in this thesis and their device characteristics followed by the parameters at which these devices were electrically stressed. Finally, Section C presents a basic description of the STEM and a brief introduction to the EDS chemical analysis process.

A. FUNDAMENTALS OF THE GAN POWER HEMT

1. GaN HEMT

The GaN HEMT takes advantage of the intrinsically superior performance of GaN while utilizing a secondary effect of lattice mismatch, which occurs at the interface between GaN and (Al, Ga)N alloys of varying Al composition. This lattice mismatch between two layers of GaN and (Al, Ga)N creates a lattice strain thus generating a charge via the piezoelectric effect as discussed in [8]. The resulting charge is proportional to the mole fraction x of Al in the $Al_xGa_{1-x}N$ material where x must be less than 30 percent [4]. Polarization charge is produced at the heterojunction between the two layers. Free electrons concentrate near the polarization region to electrostatically screen the polarization charge, creating a two dimensional gas (2DEG) region at the GaN/(Al, Ga)N interface [11],[13]. The 2DEG region is visible in Figure 1 and denoted by the dotted line.

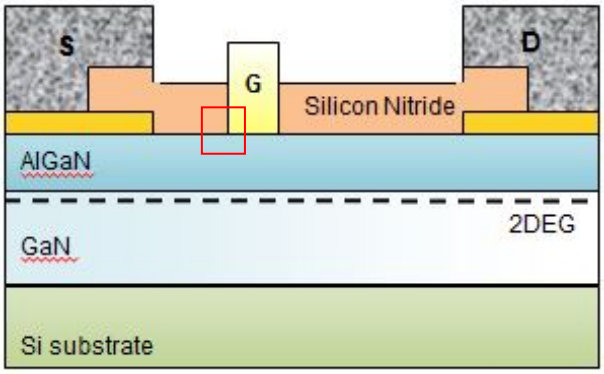

Figure 1. GaN HEMT with focus area highlighted and material layer types identified (from [15]).

The piezoelectric effect along with the spontaneous polarization of the (Al, Ga)N /GaN interface allows the device to achieve sheet carrier densities approaching $2x10^{13}cm^2$ leading to devices with low on-state resistance [4]. The bandgap of the interface between the GaN and (Al,Ga)N layers are shown in Figure 2. A gate voltage can be applied above the (Al,Ga)N barrier layer to control the sheet concentration level.

The GaN HEMT uses the channel forming the 2DEG at the (Al, Ga)N /GaN interface with an applied gate voltage to be able to create a field effect transistor (FET) [4].

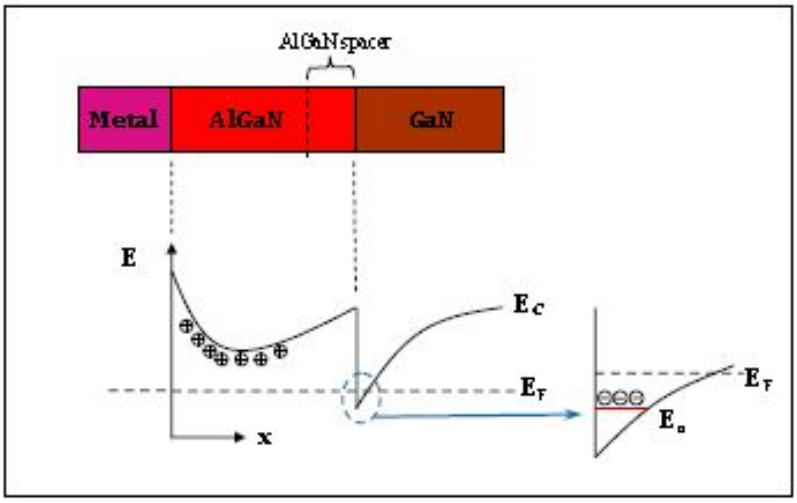

Figure 2. Energy Band diagram displaying 2DEG area (from [9]).

1. GaN HEMT Processing

a. Epitaxial growth of GaN on Si Substrate

As stated in the introduction, bulk GaN is not normally used for GaN device fabrication due to high costs. Thus, GaN HEMTs are grown hetero-epitaxially through deposition processes. There are several material layers comprising a GaN-on-Si HEMT structure. The hetero-epitaxial layer starts at the Si substrate/Aluminum nitride (AlN) interface and continues to the GaN cap layer just above the (Al, Ga)N layer, shown in Figure 3. Following the epitaxial layer metallization disposition forms the source, drain and gate contacts. A layer made of silicon nitride (Si_3N_4) is grown atop the device, creating a passivation layer on the surface to improve device performance.

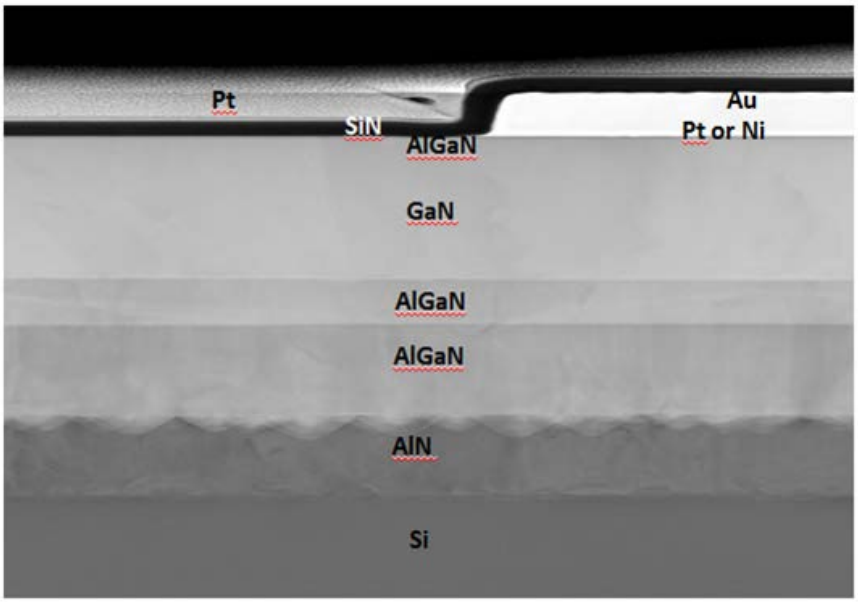

Figure 3. SEM image of cross section of the HEMT focused at the gate edge from Figure 2 denoted by the red box.

The AlN nucleation layer acts as a bonding layer between the Si substrate and the GaN layer to avoid a high coefficient of thermal expansion (CTE) mismatch between the Si and the GaN. This AlN layer prevents defects from arising during the high temperature growth procedure [4]. As seen in Figure 3, the layers furthest away from the Si substrate in the SEM image of the buffer layers shows the lattice strain lessens as the growth continues upwards. In addition, there are also far less visible dislocations in the GaN layer versus the AlN layer.

The two (Al, Ga)N layers following the nucleation layer are considered buffer layers to further reduce the strain of the active GaN layer. The decreasing concentration of visual dislocations between the two buffer layers is illustrated in Figure 3. The CTE mismatch between (Al, Ga)N and GaN layers is even lower, providing for a more stable and reliable device. Specifically, these layers reduce the leakage current through the GaN buffer, resulting in overall higher device efficiency and reliability.

After the buffer layers, the active GaN region that will compose the device area is grown, followed by the growth of a far thinner (20 nm) (Al,Ga)N layer. As previously

discussed above, the reason for the (Al, Ga)N layer grown on GaN is to induce the formation of a 2DEG channel through lattice strain at the hetero-junction.

Nominally, the vertical growth of the epitaxial regions is finalized with a GaN protective cap above the (Al,Ga)N region shown in Figure 3. This layer is very thin and important to ensure proper device functionality. This thin layer seals off hanging bonds of the (Al, Ga)N layer effectively "healing" the surface. Second, the layer increases the effective Schottky barrier height reducing gate leakage currents. Note the top GaN layer can act as a passivation layer when it is thick enough, precluding the need for a Si_3N_4 passivation layer [4].

b. HEMT Device Structure

The device structure for the HEMT is relatively simple, as seen in Figure 2. Drain, source and gate contact metals are deposited utilizing an electron beam evaporation method. A Si_3N_4 passivation layer is deposited next while still leaving an area open for the gate. Si_3N_4 is widely the favored material for the passivation layer. Some devices are unpassivated but this lack of passivation layer can lead to a buildup of negative traps causing a "virtual gate" phenomenon and reducing the drain current and power performance [16].

Despite its simplicity, there are nuances in the GaN HEMT device-level fabrication process that arise and could be the cause of defects. For example, the source and drain are patterned with a combination of titanium, aluminum (Al), nickel (Ni) and gold (Au). One aspect of the source and drain depositions is the necessity of high temperatures of around 850°C for 30s in an annealing step, which subjects the device to the diffusion of the contact metals through the device structure [4]. One option that could help to mitigate the exposure to the rest of the device would be to have a protective layer deposited before the source and drain.

B. NAVAL RESEARCH LABORATORY DEVICE

1. Unstressed Device Characteristics

The devices analyzed in this thesis were provided by the Naval Research Laboratory (NRL) and fabricated on an epitaxially grown GaN-on-Si substrate from Nitronex, Inc. The basic design of the device is similar to that shown in Figure 2. The devices have a 17nm (Al, Ga)N layer followed by a 2nm GaN protective cap. Pt/Au and Ni/Au gated devices were fabricated for these experiments. The Pt and Ni gate metal layers are beneath the Au layer. The passivation layer is of type Si_3N_4, as previously discussed earlier in Section II.A. Both Pt and Ni gated devices were used to investigate any changes in reliability. Device parameters for both device designs are found in Table 2.

Table 2. Device parameters for unstressed NRL GaN HEMTs (from [15]).

	Ni-gate	Pt-gate
R_{SH} (Ω/□)	508	
μ (cm^2/V-s)	1430	
N_{SH} (cm^{-2})	$8.64x10^{12}$	
$I_{DS,MAX}$ (A/mm)	.195	.162
$I_{DS,MIN}$ (A/mm)	$5.86x10^{-4}$	$1.98x10^{-4}$
I_G (A)	$-2.54x10^{-5}$	$-1.03x10^{-5}$
R_{ON} (Ω-mm)	26.4	21.5
V_T (V)	-1.90	-1.73
$V_{BR,GATE}$ (V)	122	121

2. Electrically Stressed Device Parameters

Previous work on the reliability of GaN HEMT device structures has identified several physical mechanisms of device level failure. Most pertinent among these is the

problem of drain current collapse, which is the reduction in drain current level at a given device bias point over long time periods under high drain/gate voltage stress [17]. Drain current collapse has been attributed to physical mechanisms associated with high fields beneath the gate contact. However, the specific defects associated with the failures have not been clearly identified.

The reliability of devices of both gate metallization types was tested electrically at NRL under two gate stress conditions. First, the device was placed under a stepped gate voltage stress until a 0.1mA gate current was observed, which did not correspond to irreversible failure of the device. Second, the device was stressed until the device reached catastrophic failure. The sample set in Table 3 outlines the stressing parameters of each device. Typical current leakage seen as the voltage was stepped on the gate is shown in Figure 4.

Table 3. Complete sample set of NRL devices used for analysis.

Pt		Stressed Levels	Stressed ID Number	FIB	TITAN
Fresh	NRL-10	NA	NA	Y	Y
Degraded	NRL-13	95V	R3GD15GF2DF2	Y	Y
Failed	NRL-12	135V	R3GD15GF2DF4	Y	Y
Ni					
Fresh	NRL-Ni-1	NA	NA	Y	Y
Degraded	NRL-Ni-3	130V	R3GD15GF2DF3	Y	Y
Failed	NRL-Ni-4	125V	R3GD15GF2DF4	Y	Y
Epi layer	NRL-Epi-1	NA	NA	Y	Y

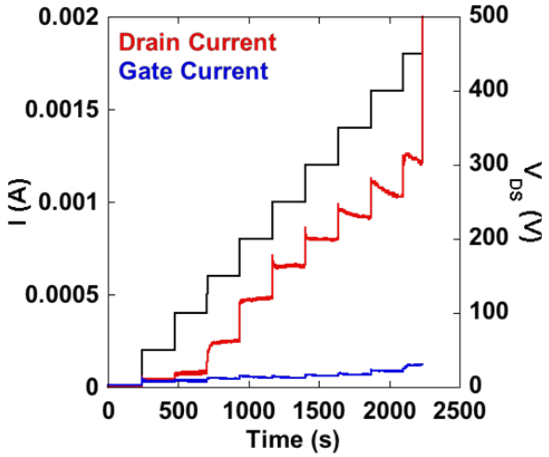

Figure 4. Current/voltage plot of the electrical stress test performed on Ni and Pt devices (from [15]).

Stressed devices were then tested for electroluminescence phenomena. Electroluminescence is the emission of light in areas of high electron-hole recombination due to a presence of charge carrier trap states in the bandgap. The wavelength of the emitted light is directly related to the energy levels of the traps. Thus, the presence of electroluminescence can be used to infer a greater chance for defects in the area in which the phenomenon occurs. Several peaks over the visible light area of the electroluminescence spectrum are observed, as seen in Figure 5. The origin of this "yellow" luminescence is discussed in [18], and is related to defects in the GaN material. Points in the device structure where the luminescence spectra was similar to that shown in Figure 5 helped to identify where our sample slices would be extracted.

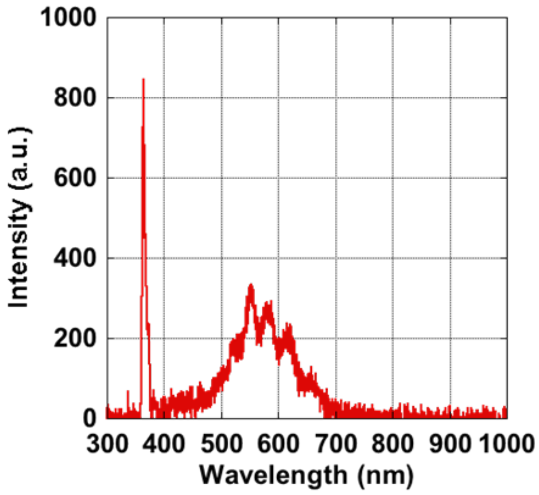

Figure 5. Wavelength intensity of defected GaN region gives rise to photoluminescence evidence (from [15]).

C. STEM AND ENERGY DISPERSIVE X-RAY SPECTROSCOPY

Transmission electron microscopy (TEM) uses an electron beam to image very thin samples at an atomic level. Electrons are emitted by an electron gun and are accelerated to high speeds. The electrons then transmit through the sample and are collected in a detector, usually a charged coupled device (CCD) camera, forming an image. The scanning transmission electron microscope (STEM) operates from the same underlying principle as the TEM does. However, the beam scans in a raster pattern forming an image over a wider area instead of focusing in one location only [19]. Note, the sample must be thin enough to ensure the electron beam passes through and scatters. The thinner the sample, the higher resolution the detector can capture. Ideally, these samples have an optimum thickness of 10nm.

Energy dispersive x-ray spectroscopy (EDS) is an analytical tool used in conjunction with a scanning transmission electron microscope (STEM) that detects the x-ray backscatter from the STEM on the sample and associates the detected x-rays to an element's energy level. While the detector is integrated into the STEM stack, additional software is needed to analyze the spectral data. This software allows the user to analyze the image or map by providing the elemental composition of the area imaged. The EDS

integrated with the Titan STEM at LBNL has the capability of detecting the lighter elements in blue as seen in Figure 6, which was crucial to our experiment.

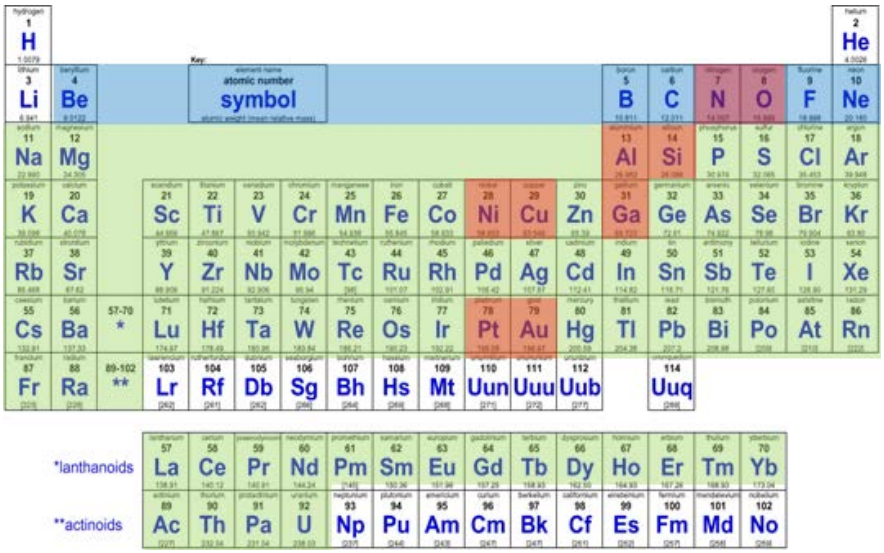

Figure 6. EDS detectable elements. The elemental table highlights the light elements in blue, elements of interest in this thesis in red and other EDS detected elements in green.

The microscope also has the ability of producing not only qualitative spectral distribution information but also quantitative data upon the total amount of material present. This thesis focuses on the qualitative information; however the samples used are thinned to approximately 10nm thick for high resolution images as well as 3-D atomic reconstruction. Due to the thin sample requirement for images as well as the need to be able to image the sample at multiple thicknesses throughout its lifecycle, a new sample preparation procedure was required and developed in this work. This new sample preparation procedure will be discussed in Chapter III.

III. SAMPLE PREPARATION

TEM imaging requires that a sample be less than 200nm thick. Traditional methods in TEM sample preparation include grinding, polishing and etching a circular sample by repeating the thinning methods focusing on the center of the circle. Once the disk breaks in the center, the inside edges are deemed thin enough for the TEM. This method works with bulk material but is not suitable for imaging the cross section of a HEMT. A new approach was required. This process was developed, designed and optimized in conjunction with Dr. Petra Specht from University of California, Berkeley.

This section describes the sample preparation procedure and begins by providing information about the location where the experiments took place and listing experimental steps required to remove a section from the device encompassing the gate using the FIB. Finally we describe how the NanoMill was used to thin this small section or sample to meet TEM requirements for image resolution.

A. LOCATION AND MACHINES USED

All sample preparation was conducted at the Lawrence Berkeley National Lab (LBNL) specifically within the National Center for Electron Microscopy Program. The center is a national user facility with specific time slots allowed per month. Given the amount of time taken to produce and analyze one sample, the sample preparation process required a focus on efficiency as well as consistency to ensure the entire time slot was used as best as possible.

Some of the machines/microscopes used for this sample preparation technique are currently or are scheduled to arrive at NPS. Currently NPS has a FIB with Pt source capable of a sample lift out procedure. A TEM with a light element EDS detector for chemical analysis as well as the Bruker© chemical analysis is also planned for installation. Having these capabilities at NPS will allow for a larger amount of samples to be made in a much shorter amount of time, as NPS does not have the traffic or user limits that a national user facility does. At LBNL, two time sessions per month per machine are

authorized per user, meaning only two samples could be produced per month barring no machine failure or sample breakage.

The sample set in Table 4 was used as a guide for our experiments. We isolated the cutting area to be the same for each sample, making sure that we cut away the entire gate width within each sample. Each sample went through the same sample preparation procedures to minimize inconsistent data. The focused ion beam was used to cut out each sample followed by the NanoMill to achieve a thickness less than 150nm. Finally, we used the energy dispersive spectrometry (EDS) detector to image and chemically analyze the sample area.

B. FOCUSED ION BEAM MILLING AND LIFTOUT

The FIB has multi-tool capabilities with SEM imaging, an Oxford Instruments OmniProbe© manipulator, chemical deposition as well as ion etching. The instrument is seen in Figure 7. Therefore the sample under preparation can be etched at the micrometer level. The tight control over the emission rate of ions from the source means the ability to keep the ion current low enough to minimize further damage to the sample. The FIB, combined with a fine control sample manipulation system (the OmniProbe) allows performing a lift out where the 20µm long sample is removed and welded to a copper port for further thinning, transportation and evaluation.

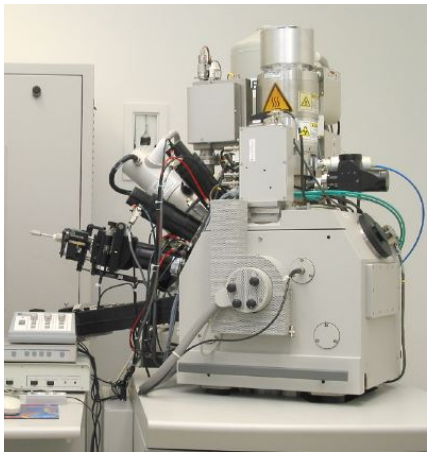

Figure 7. FIB with OmniProbe on the left with the SEM stack on the top.

1. Initial Setup

The sample holder inside the FIB rotates and moves and therefore the integrated circuit (IC) needs to be properly secured to the mount prior to loading into the machine. Carbon tape was used to secure the (IC) to the mount because permanent adhesion of the IC to the mount was not feasible. In order to make sure that the IC was more secure, the ends of the tape were rolled up to the edge of the IC. The sample that would be cut from the IC was required to be mounted. The chosen mount was a five fingered copper port. In a later process, the EDS TEM sample holder will have three metal options, copper, molybdenum and nickel. A five fingered port was chosen in order to provide protection during transportation as well as the metal type. The copper five fingered port was mounted fingers pointed straight up as seen in Figure 8.

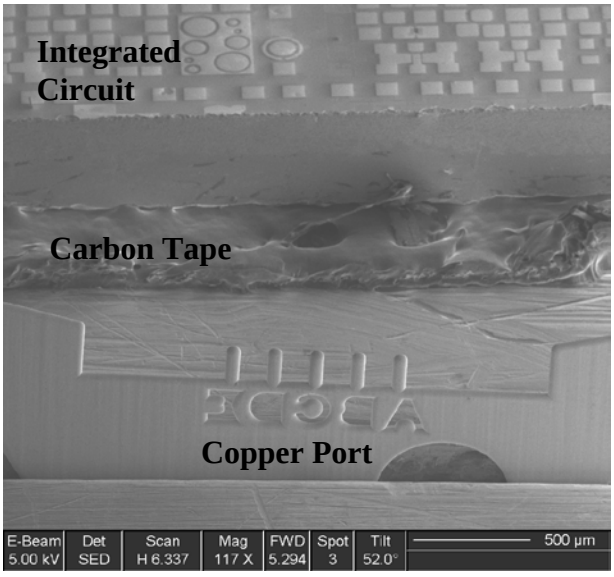

Figure 8. SEM image of five fingered copper port used to hold the lamella with the IC in the background with rolled carbon tape securing the IC.

When the mounting process was complete, the sample was loaded into the SEM chamber. The electronic beam (E-beam) voltage was set to 5kV with a spot size of three and the ion beam (I-beam) current level to 10ρA. The imaging mode was set to E-beam and was used on “continuous scanning” to bring our IC into focus by adjusting the Z-height. We made sure to adjust our focus to an area not being cut as to minimize inducing

degradation to the device. Once we achieved a clear picture as shown in Figure 9, the tilt angle was adjusted from 10° to 52° in order to achieve the eucentric height. Eucentric height is the working distance in the z-axis of the mounted device where focus is achieved independent of the underlying tilt angle of the sample.

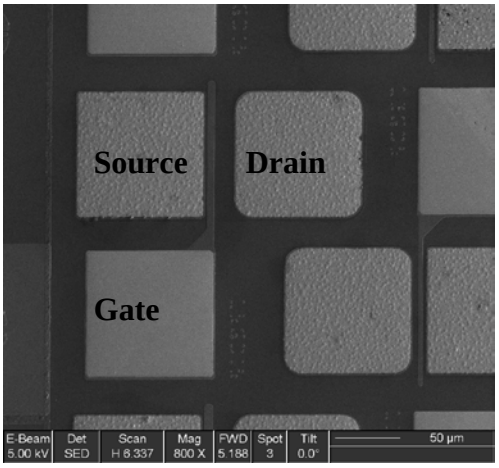

Figure 9. SEM image of properly aligned E-beam image indicating sample is at eucentric height and therefore focused.

Since the microscope was focused using the E-beam, it then needed to also be focused using the I-beam. The E-beam and I-beam images were compared until both images were of the same area. Adjustments were made to the I-beam by positioning the beam itself. Since the I-beam and E-beam are mounted at different angles within the machine, making sure that both are aligned with each other gave an overall three dimensional image, which was used for moving the sample and tools into the correct position.

2. Sample Protection

Once the microscope and IC were properly focused, the sample preparation process began. The particular device within the IC was chosen and focused upon. The next step in the procedure involved beginning milling with the I-beam. Note that the area along the gate where the sample would be cut out required protection from the high current I-beam, which came from depositing a Pt layer at low current to act as a shield.

A box covering the source and the width of the gate of dimensions approximately 20µm long, 2µm wide and only 0.1µm thick was selected as the target area for Pt deposition. The I-beam current was set to 10ρA in order to create a purer, higher density Pt base with the least possible damage to the device. Two additional layers of Pt with thicknesses of 0.35µm and 0.55µm at 50ρA and 100ρA respectively were subsequently added. The three completed layers are seen in Figure 10.

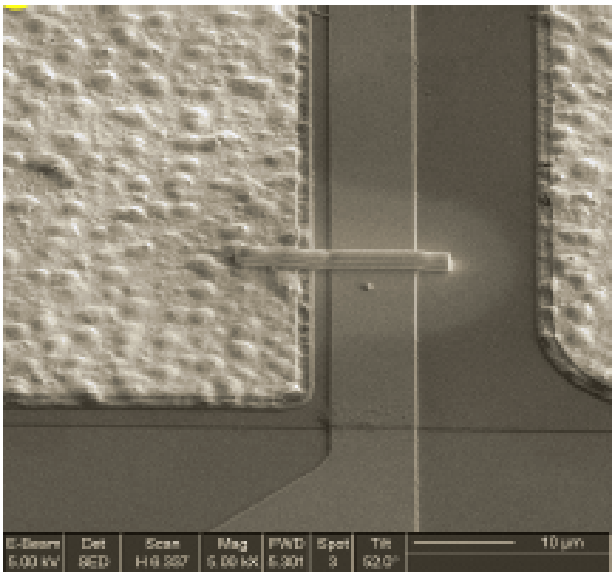

Figure 10. SEM image of 1µm Pt protective layer over the device source edge and gate.

The Pt shield placed over the source edge and the gate served to identify where the cut is to be made, and to protect the sample area from further damage during the I-beam etching/cutting process.

3. Ion Cutting Methodology

With the sample area identified and protected, the area surrounding the sample needed to be removed so that the sample could be lifted out. The cutting process is a balance of cutting time versus ion radiation exposure. The higher the ion current, the faster the FIB cuts the device. Note the sample needed to be prepared for the lift out by cutting away three sides around the Pt shield. As a result a level of 1000ρA was initially

chosen to cut away two 5µm wedge shaped trenches above and below the sample, as seen in Figure 11. The closest edge of the trench cut was chosen to be approximately 2µm away from the Pt shield in order to keep the higher beam current levels from causing additional degradation as well as providing a buffer area should the I-beam shift slightly while cutting. Each large trench took approximately 40min to cut.

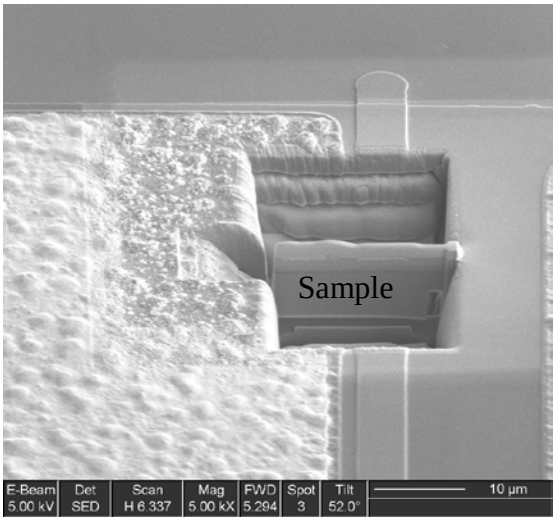

Figure 11. SEM image of 5µm deep trenches etched around the sample.

Next, a smaller third trench was cut to allow for the OmniProbe manipulator to have the room to be placed in position next to the sample. The smaller third trench is seen in Figure 11. The small trench is cut at an angle perpendicular to the other two wedges but at the same amperage and depth as the first two wedges. The other requirement for the wedge was its placement, as the third trench needed to overlap both larger wedges to free the sample completely on three sides.

After cutting the larger trenches, debris built up along the surface between the hole and the deposited Pt. The debris made it difficult to distinguish from the deposited Pt therefore each side was cleaned with 300ρA of ion radiation. One final cut was needed to free the bottom of the sample. The shape shown in Figure 12 was made to create the undercut. We remained mindful that the box labeled “2” in Figure 12 extended past the sample edge as well as overlapped with block labeled “1.” Block “1” was aligned to begin at the notch created in the earlier cleaning series. In addition, the IC was tilted by

an angle of 45° from the original angle in order for the I-beam to be in the correct position. The machine was also adjusted from serial mode to parallel mode in order to cut both boxes simultaneously. The sample with the undercut is seen in Figure 11. The undercut in Figure 11 is the same shape as the combined boxes from Figure 12 but upside down. There is now a small bridge connecting the sample to the IC after the undercut. The sample was tilted back to the 52° after the undercut was made to ensure the location of the I-beam would be directly above the sample and not at an angle.

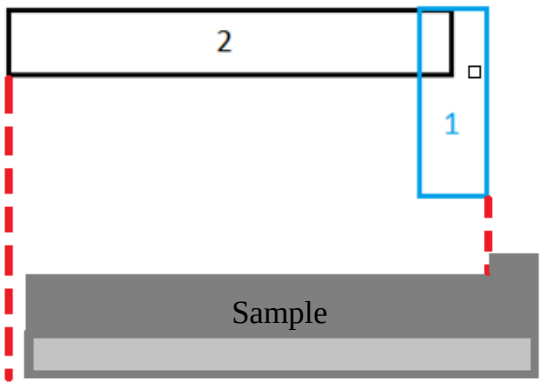

Figure 12. Schematic for parallel FIB undercut layout.

4. Lift Out Method

The sample at this point of cleaning is approximately 1µm thick and is ready to be mounted to the port. The small lateral trench etch to the side of the device discussed in Section III.B.3 and depicted in Figure 11 was made for the OmniProbe. Next, the sample was lowered and the OmniProbe and Pt source were brought into the working area. The OmniProbe must be sharp and free of debris that a previous user may have left behind so a strong Pt weld may be created between the surface of the OmniProbe and the side of the sample.

Once the probe was clean, the sample was slowly brought into focus and the probe was carefully placed against the edge of the sample. The probe was required to touch the sample in order to achieve a proper weld, but the speed at which the probe was positioned was chosen to be very slow so as to not break the sample. The OmniProbe positioning when bringing it into contact with the sample is shown in Figure 13. Note the

actual contact between the probe and the sample is not shown but Figure 13 does illustrate what the probe tip should look like as it is being positioned in relation to the sample.

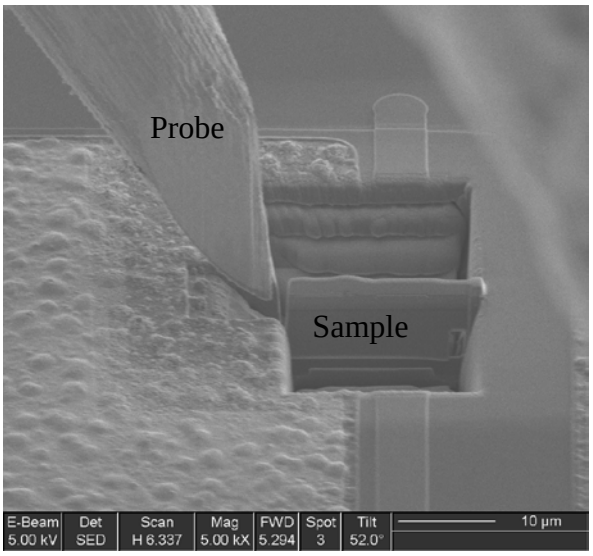

Figure 13. SEM image of OmniProbe shown in position for welding the sample.

Once the probe is in contact with the sample, the Pt source was used to weld the sample to the probe. Once the probe had a thick weld of approximately 0.1µm, we cut away the final edge of the sample freeing it from the IC. The IC was then slowly lowered so the lamella (sample) was present and securely fastened onto the probe. Figure 14 shows what the lamella looks like once it has been lifted out of the IC.

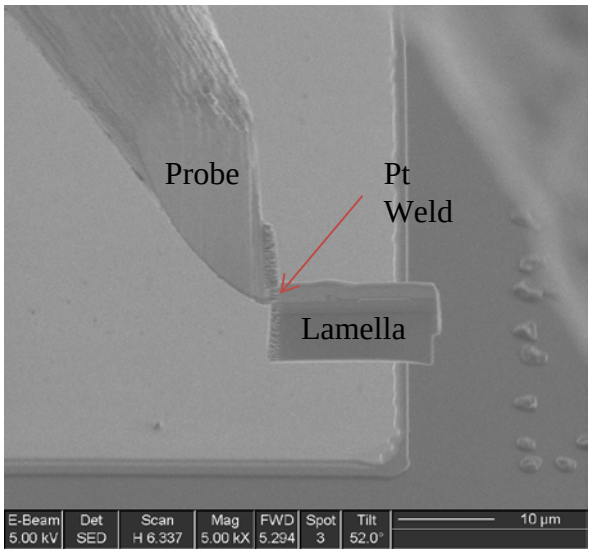

Figure 14. SEM image of lamella welded onto the probe with Pt.

5. Mounting

The lamella needed to be welded to the copper port to be transferred to the TEM and the port needed to be prepped to be able to fit the lamella for welding. We removed the OmniProbe from view and then widened our magnification to find the five fingered port seen in Figure 15.

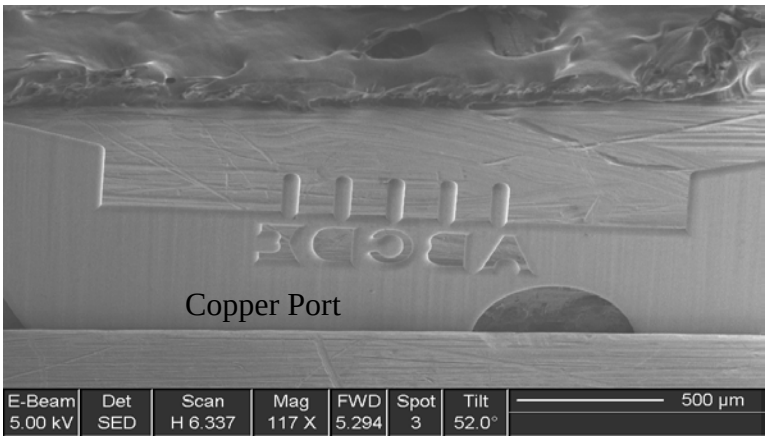

Figure 15. SEM image of the copper port properly mounted and in correct field of view. The orientation of the port is the same for every sample.

Once the port is in view, each lamella prepared was consistently mounted onto the same port. We chose to mount the lamella to port C for added protection when handling as well as for ease of locating the port in the TEM in later sample analysis. The lamella was mounted on the open side of the C port because the closed side could be confused with the curved edge of port D. We also needed to adjust and find the eucentric height as the port is at a different height than the IC. We adjusted our tilt to 0° and zoomed into the port.

At that point, a trench was made into the top of the port denoted by a green box in Figure 16, and is approximately 1.5µm deep. The opening was chosen to measure twice the width of the sample in order to safely accommodate the lamella. Once the port was prepped for the lamella, we brought the lamella back into the field of view. The port was slowly raised up to the lamella and then carefully placed into the trench in the port. The port in the process of rising to meet the lamella is shown in Figure 17. The trench made from the schematic in Figure 16 on the left side of the port is also visible in Figure 17 creating a pocket or envelope for the lamella to fit.

Figure 16. Schematic of top down view of one port with green box depicting where cut should be placed.

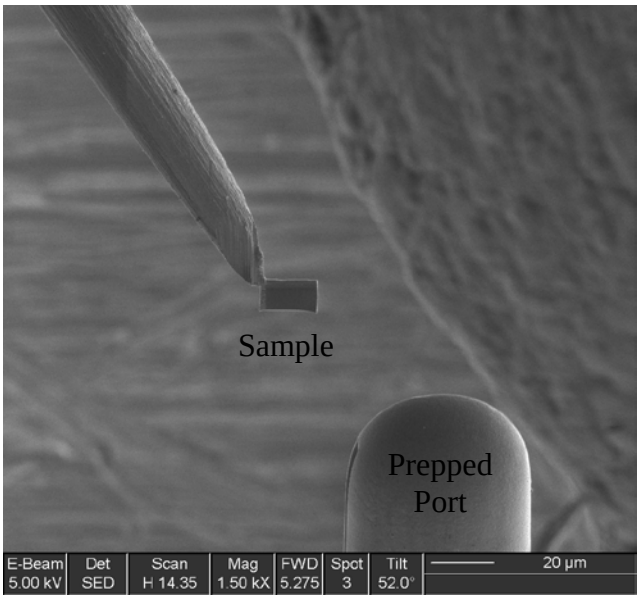

Figure 17. SEM image of welded sample moving into position to the prepped port.

Once the lamella was docked into the pocket, the top edge of the lamella was welded to the port using the Pt source. This weld was the first of three major welds, but was mechanically secure enough to free the OmniProbe from the lamella. Once the lamella was attached to the port, the port was tilted to 30° and another weld made to approximately 0.1µm thick along the front of the port. To make the final weld along the backside of the port, the port was rotated by 180°. We applied another Pt weld at a similar thickness to the backside of the port.

6. Thinning

At this point, the sample was still approximately 1µm thick at the widest point. Due to the requirements of TEM imaging, the sample needed to be further thinned to approximately 250nm-400nm thick. The FIB/SEM was again used to perform the thinning of the sample. This thinning process is very time consuming as the I-beam at this step was only at a current 100ρA to prevent damage to the lamella. Once the lamella is thinned on both sides, we performed one more cleaning on the tip of the lamella to clear any remaining debris.

The welding to the port and an image of the lamella after the thinning process is shown in Figure 18 for a device with no degradation. Note the different epitaxial layers

are clearly defined in this figure. Large areas of degradation were not visible in the fresh devices, but were present in the stressed devices. The beginning of the thinning process was started far enough away from the weld as to not cut away any previous welding that was done.

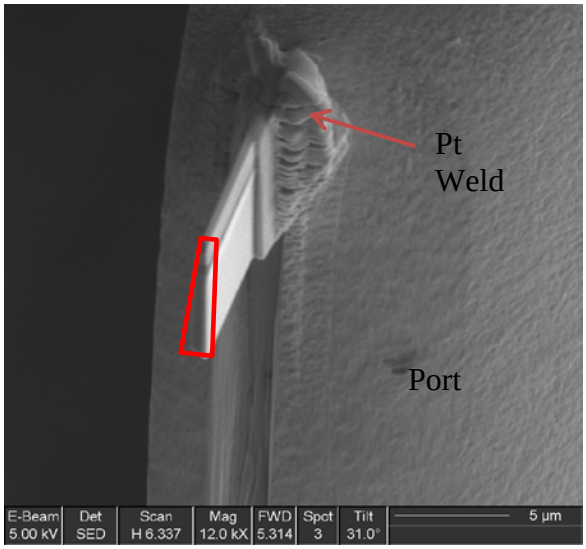

Figure 18. Final SEM image of the sample welded to the port. The top of the device is much thinner than the bottom creating a trapezoidal shape.

At this point, only the top area of the lamella was used to gauge its thickness, as the FIB mills progressively less of the lamella towards the base, forming a trapezoidal shape. The shape of the finished lamella can be seen in Figure 18. Since the top of the structure is the thinnest portion, it was chosen to correspond to the point closest to the active layer. Thus all further analysis was taken near the top of the sample.

C. ION MILL

The role of the NanoMill is to further thin the lamella down using a lower voltage than the FIB to approximately 150nm in order to meet the thickness requirements for the TEM. Note that the sample should be less than 200nm to insure the best imaging results. This NanoMill machine is more accurate than the FIB and induces less degradation by milling at lower voltage. At the lower rate, the time to thin is also longer. The NanoMill seen in Figure 19 was run for approximately 15–20 minutes at energy of 700eV and a

desired emission current of 130µA. This step was performed before each session to help the beam current reach approximately 130ρA as well as clean the tip of the gun to ensure consistent results across all samples.

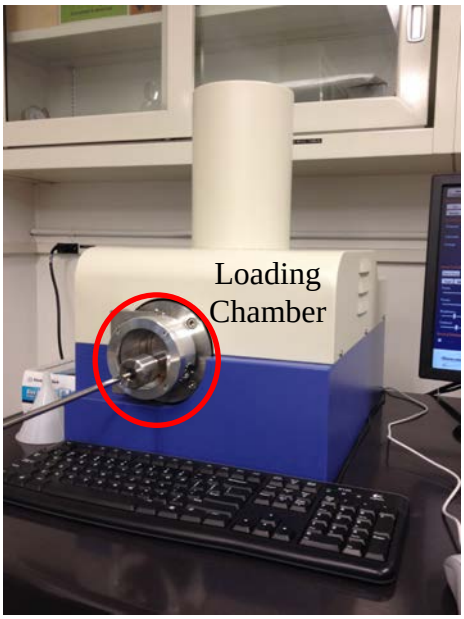

Figure 19. NanoMill machine with loading area in silver. There is a two-stage vacuum present, one to allow for the loading area and the other for the chamber itself.

Once the sample was loaded, we identified our lamella on the monitor screen as seen in Figure 20. We adjusted the angle of rotation slightly so that the lamella was level. We adjusted the tilt angle to 7° to make sure that we were only milling the top area of the lamella and maintaining the structural integrity of the lamella. We defined our milling area by adjusting the ΔX and ΔY parameters to be 15µm and 10µm respectively.

Figure 20. NanoMill control screen showing parameters for the milling process and monitor screen.

Once the milling area was defined, we needed to define our milling parameters. We set the energy to 900eV and the desired emission current to 180µA. The milling time was set to 40 minutes. In order to have consistent results with respect to milling rates, the actual beam amperage was around 120–130ρA.

Once the milling process was complete we adjusted the tilt to -7°, shown in Figure 20 and milled for another 40 minutes. This angle allowed us to mill the other side of the top of the lamella. Alternating tilt angles reduced the amount of the Pt shield but also created a bit of a roof shape at the top of the lamella. By milling in this fashion, we were able to save time by only milling the area with the device and not mill the excess silicon substrate.

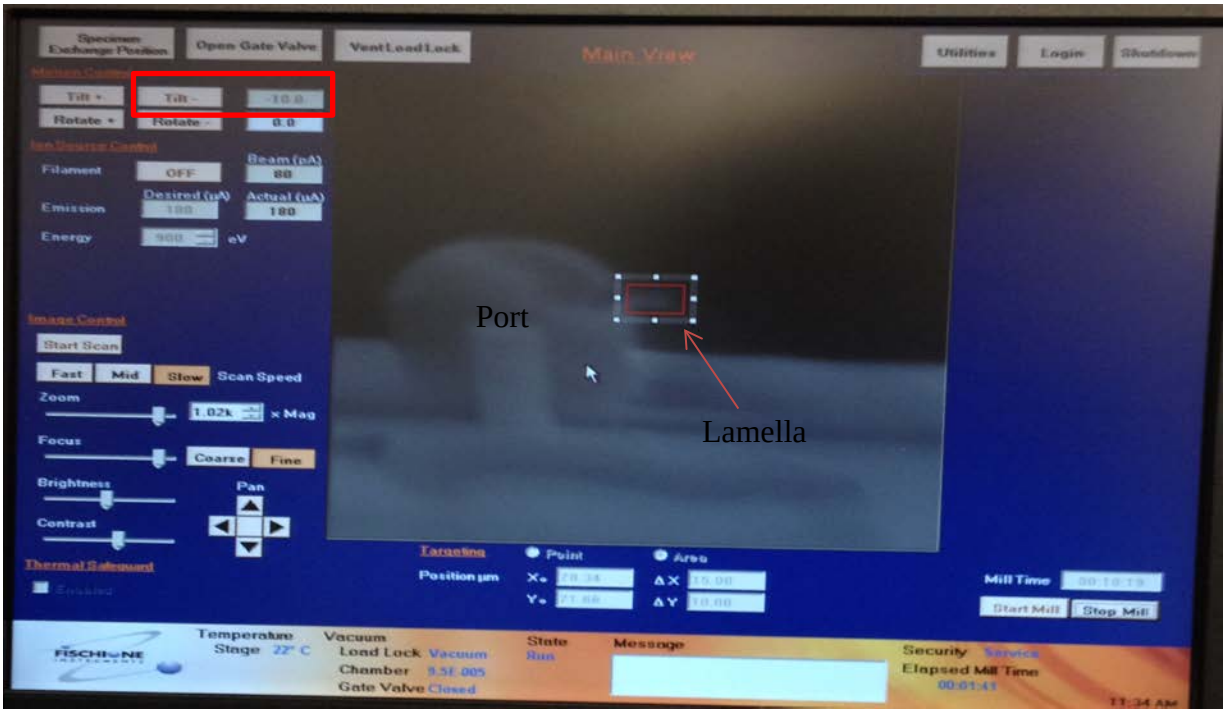

Figure 21. NanoMill control screen depicting the -10° tilt angle and underside of the port.

The tilt angle was again adjusted to 10° and milled for 10 minutes keeping energy, current levels, and milling area the same. The process was repeated at a tilt angle of -10°, as seen in Figure 21. The negative tilt angle grazes the top area focusing on thinning near the top of the lamella from the other side. Using positive and negative tilt angles create a roof shape on top of the sample thus only thinning the active region of the device but not compromising the structural integrity of the sample. Milling for a total of 100 minutes in this +7/-7/+10/-10 tilt angle fashion was found to reduce the sample thickness to approximately 100nm. We also found that the milling rate largely depended on the actual amperage staying in the 120–130ρA range as it varies throughout the milling process. We also noted the effective milling rate was not noticeable if the amperage fell below 110ρA. Given this microscope's resolution limitations, we were unable to measure the lamella in the machine. The thickness measurements were performed using the TEM prior to the analysis sessions.

D. RESULTANT SAMPLE AND COMPARISION TO PREVIOUS WORK

The sample/lamella after the NanoMill thinning process is approximately 100nm thick, which meets the TEM minimum requirement of 200nm for an image. The thickness of the device could not be measured in the NanoMill due to its internal microscope's limitations thus making identifying an approximate milling rate very important. The last measurement that can be taken is in the FIB, as seen in Figure 22.

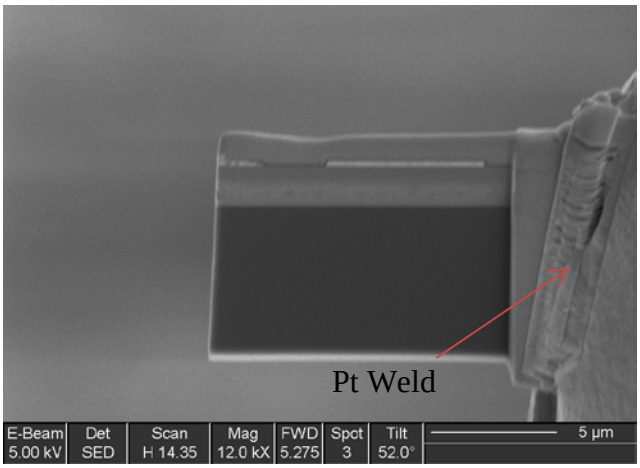

Figure 22. SEM image of sample properly welded, thinned and mounted to the port.

A similar sample preparation technique discussed by Nan in [20] used a lift out procedure with the FIB. However, the author noticed a 30nm amorphous layer created in their sample due to FIB damage. Note this damaged region created by the FIB would not be acceptable for our samples. Finally, Nan's work did not mention the use of an ion mill. Due to early TEM high resolution images taken of these seven samples, the samples at 10nm thick do contain crystalline structures meaning that the sample preparation procedure is successful in limiting dislocations in the sample. At that point the samples obtained were now ready for the first TEM image and EDS data analysis, as discussed next in Chapter IV.

IV. RESULTS

This section discusses how the samples created were chemically analyzed. The sample set contains seven samples. Section A focuses on the epitaxial layer substrate. Section B looks at the three Pt samples and analyzes where different chemical elements are found along the gate edge. Section C contains the data analysis for the three Ni samples. Finally, Section D compares the data from the previous section to discern trends between the seven samples.

The TITAN 300 STEM allowed us to focus on the source side gate edge and analyze the elements present due to process and stressing of these devices. Elemental analysis of GaN HEMTs has not been investigated in this method before and can serve to identify processing and electrical stressing defects. Using the Bruker© EDS software, data collected from the STEM/EDS system was analyzed and interpreted. The elements chosen to be focused on are based on the device layers fabricated and material information provided by NRL and Nitronex as well as the spectral data peaks within the software identifying the present elements.

Four line scans along the gate edge of the device were taken from the data. Figure 23 shows four vertical black lines across the device to represent where the data was taken along with labels corresponding to the location: Active layer, Dip, Foot, and Gate. The data set in Table 4 describes the four line scans from Figure 23 taken across the six device sample lamellas as well as two additional line scans across the pre-fabricated epitaxial layer. Each element within the line scan data is a count percentage normalized to 100 over the entire image. Interpreting a quantity of each element cannot be accomplished until the sample is electron transparent at approximately 10nm. The identification of elements present in a thicker (100nm) sample was needed before subsequent thinning steps so as not burn up the entire sample at the last step without acquiring data throughout the procedure.

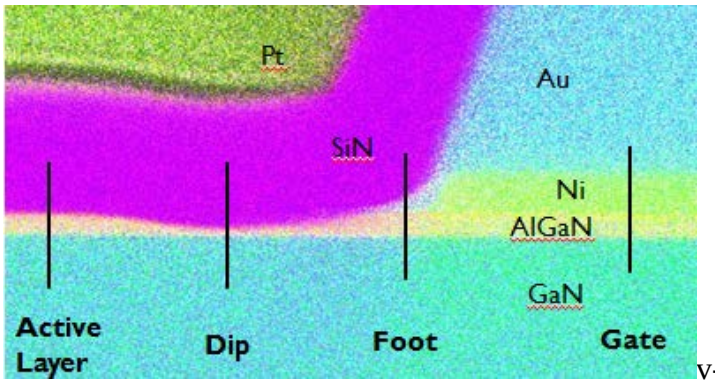

v-

Figure 23. Ni/Au gate edge with the four line scan areas labeled.

Table 4. Line scan chart for all samples analyzed.

PT Devices	Gate	Foot	Dip	Active Layer
Fresh	X	X	X	X
Degraded	X	X	X	X
Failed	X	X	X	X

Ni Device	Gate	Foot	Dip	Active Layer
Fresh	X	X	X	X
Degraded	X	X	X	x
Failed	X	X	X	X

Epi layer	X	X		

A. EPI LAYER

We initially chose to look more closely at the original epitaxial layer made by Nitronex, Inc. provided by NRL to see if the lack of 2nm GaN cap was due to processing or if the protective GaN cap was not present from the beginning. In Figure 24 (b), we see that there is a peak in the gallium (Ga) right at about 5nm into the line scan data. Graph (a) in Figure 24 has a slight Ga concentration increase near the 10nm area. Results shown here validate that the 2nm GaN cap was present before the devices were grown on top of the substrate layer.

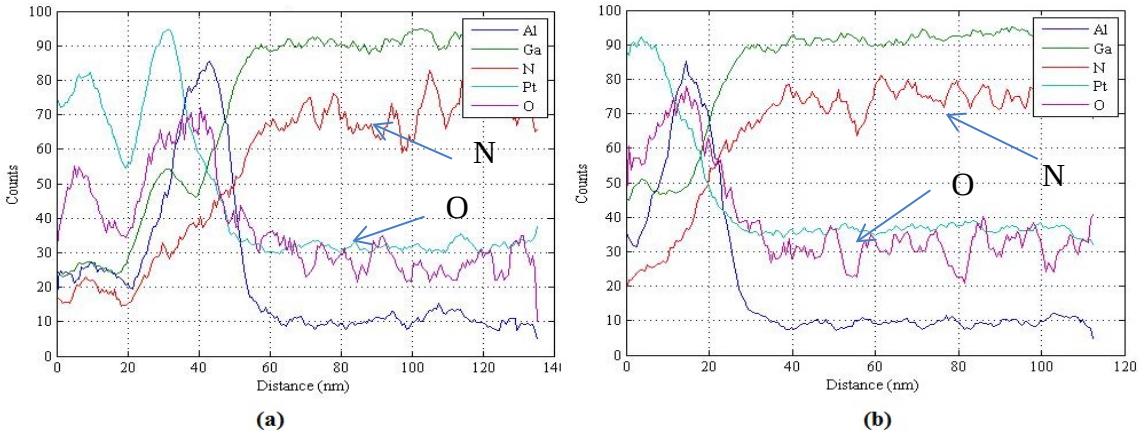

Figure 24. Hetero-epitaxial layer line scan plots showing a normalized percentage count for each element. (a) and (b) were taken from the same sample in two different locations

The other noticeable element in Figure 24 is the presence of oxygen. The substrate should not have any oxygen present because the fabrication of the epitaxial layers was grown in vacuum. However, analysis of this substrate was not completed until a year after being placed in storage, which suggests that an oxide accumulated over that time. In [18], the presence of oxygen unintentionally doping the (Al, Ga)N layer is discussed.

B. PT DEVICES

There were three (fresh, degraded and failed) Pt devices that were analyzed in the four separate line scan areas. We looked at the source side of the gate on all devices due to the electroluminescence image on the stressed devices. The three Pt samples made using the procedure discussed in Chapter III were individually placed in the TEM with EDS detector for chemical analysis. The line scans were then taken and the data analyzed.

1. Fresh

The fresh device did not undergo any electrical stressing. We used this device to help identify any defects due to processing as well as to set the standard or baseline for comparison of the stressed devices. Figure 25 focuses on the area where the data was

taken. The colors present in each box represents where that element is found within the standard STEM High-Angle Annular Dark-Field (HAADF) image (the black and white image in the top left position). The last image labeled Composite is the composition of all seven elements present within the STEM image.

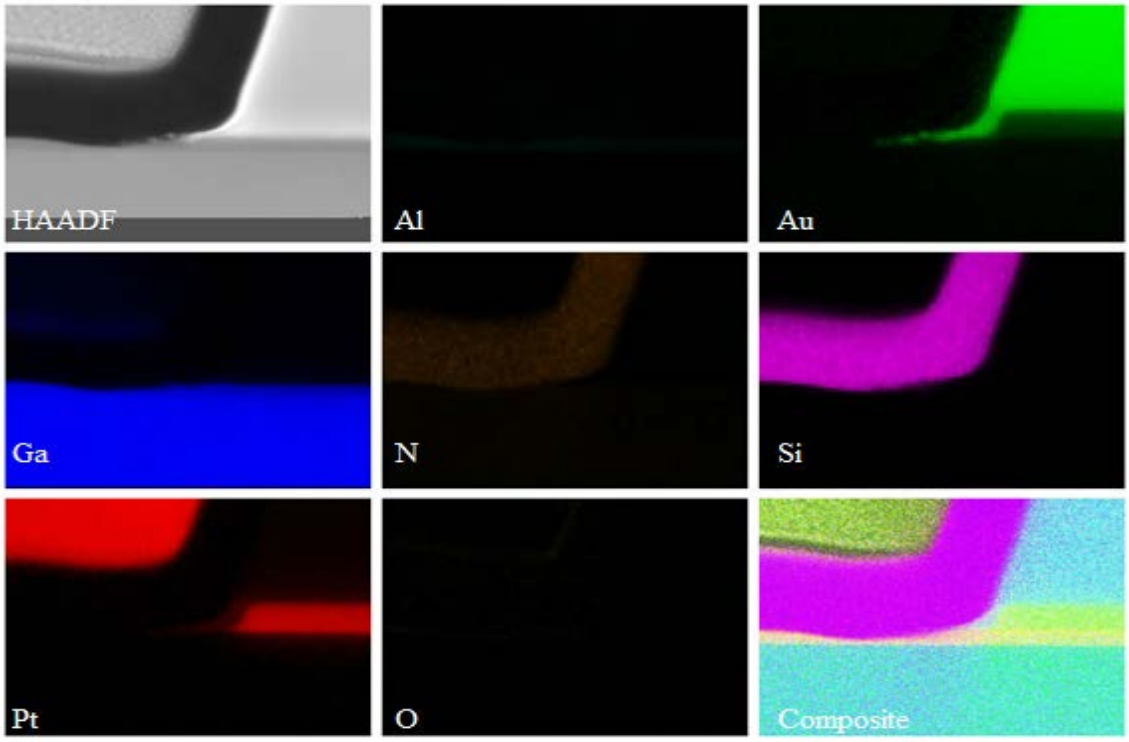

Figure 25. STEM image from the EDS of the fresh Pt gated device broken into each element of focus.

The elemental x-ray spectrum is shown in Figure 26. As the EDS scans through the STEM image, it tracks the number of photon counts corresponding to each energy level. When we analyze the data of the line scans, we use both the elemental images in Figure 25 as well as the spectral data in Figure 26 to help determine any artifacts or outlying information. Copper (Cu) is present in every spectrum due to the copper port the lamella is mounted in and the sample holder that the port is sitting on within the microscope. Each spike is also labeled with one of the seven elements listed in Figure 24.

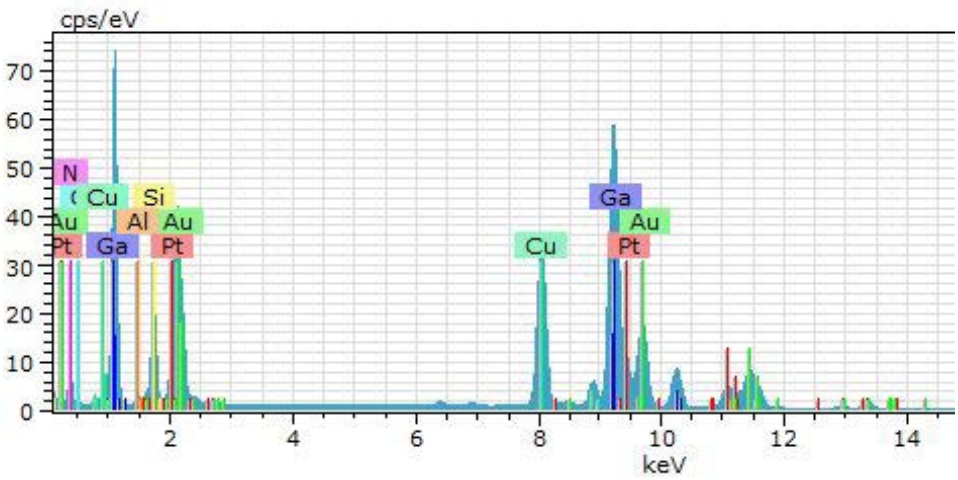

Figure 26. Elemental spectrum display of electron volts versus photon counts of the fresh Pt sample. The peaks in the spectrum correspond to individual elements present in imaged area.

Note that the height of each peak is important in determining the quantity of each element present in the data. In addition, Ga and Pt also have very close electrical spectrum energy levels and therefore their spikes can sometimes creep and distort the data. We found that the Pt tends to follow the Ga concentration because the peaks are so close together in the spectral data. This following is an artifact and was minimized in the line scan data plots after the raw data was analyzed.

Note the line scan data is normalized to a percentage against each individual element; therefore the height of the lines can be misleading as the height of each element can only be compared to itself. Chemical concentration information is not displayed but can only identify that the EDS detected a presence of elements. We can see how far the element diffuses into another layer but cannot yet say how much of each element is present.

When we looked at the gate of the fresh device we expected to see a layer of Au, followed by Pt, a thin 2nm GaN layer, (Al, Ga)N and finally a GaN layer. We noticed every line scan did not have the 2nm thin GaN layer present due to a lack of a Ga peak before the increase of Al. Oxygen was unexpectedly present in all line scans. Figure 27 has oxygen present in both the Au and Pt areas. There might be aluminum oxide (AlO_x)

diffusion into the (Al, Ga)N layer due to the spike in oxygen prior to the Al rise. The (Al, Ga)N and GaN layers appear as expected due to the other elements not having a high percentage count.

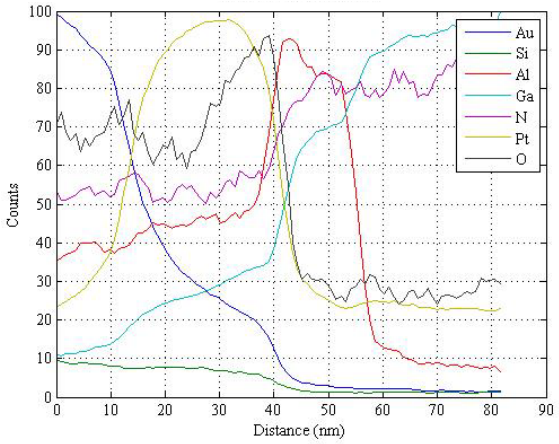

Figure 27. Line scan data from the fresh Pt gate line scan depicting the rise and fall of each element presence analyzed.

Moving across from gate to the active layer area, we noticed an irregular area shown in Figure 25. The gate should have a sharp drop off and sit nicely on top of the thin 2nm GaN cap. However, in all of our devices/samples we noticed this area where the gate seemed to melt or move to create a “foot.” Note the term “foot” is not technical but rather used throughout to depict this particular area on each sample.

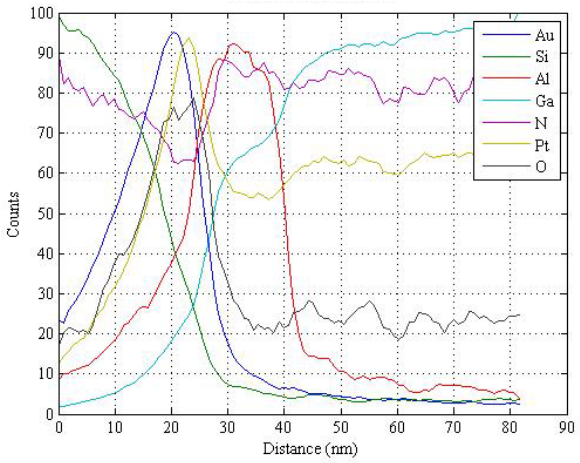

Figure 28. Line scan data from the fresh Pt foot line scan depicting the presence of each element analyzed.

We expected the foot area to have a silicon nitride (SiN) layer, a Au and or Pt area, followed by the GaN cap, (Al, Ga)N and GaN layers from the composite image seen in Figure 25 combined with the processing elemental information from NRL. However, the GaN cap layer was not present. The Si_3N_4 and GaN layers were both clear and appeared to be free of other elements diffusing into them. The foot area itself is composed of Au on top and a mix of Pt and O. The Pt data within the GaN layer is an artifact as discussed earlier due to the similar electrical spectrum information.

Continuing to the third line scan taken on this sample, we chose to focus on the area where the (Al, Ga)N layer was visually thinnest shown in Figure 23. This layer should remain constant throughout the entire IC and yet in all the devices this thinned (Al, Ga)N area is present. This area was termed the “dip” in Figure 29.

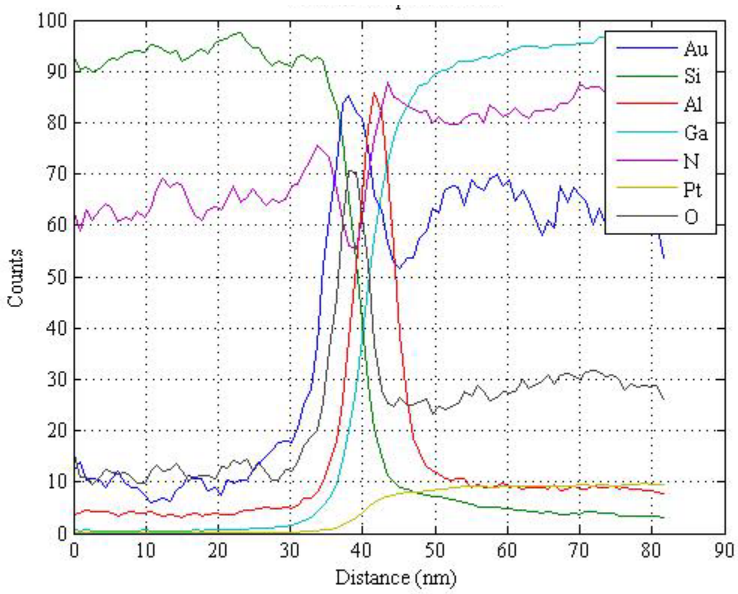

Figure 29. Line scan data from the fresh Pt dip line scan depicting the presence of each element analyzed.

We did not expect to see any dip area when these devices were analyzed for the first time. The thinned area is easily depicted in the plot shown in Figure 29 by having the Si_3N_4 layer on the left and then the GaN layer on the right. We expected to see some amount of (Al, Ga)N within the dip itself and there is a small layer present. There is however, still a presence of Au. This result indicates that Au is transported across the device diffusing outward during processing. We also noted that there is also an oxygen peak between the Si_3N_4 and the (Al, Ga)N layers.

Finally the last area analyzed was the active layer as we wanted to have a baseline far from the gate edge itself. Results shown in Figure 30 indicate there is no Au or Pt present. The Au had been present in all line scans of the fresh Pt sample with the exception of the active layer scan. The lack of Au in this line scan shows the melting effect of the Au from the gate is limited in how far Au will travel. Results also indicate there is a clear delineation between Si_3N_4, (Al, Ga)N and GaN layers. Finally, we note the oxygen peak is still present between Si_3N_4 and (Al, Ga)N layers. This peak of oxygen appears consistently between these layers.

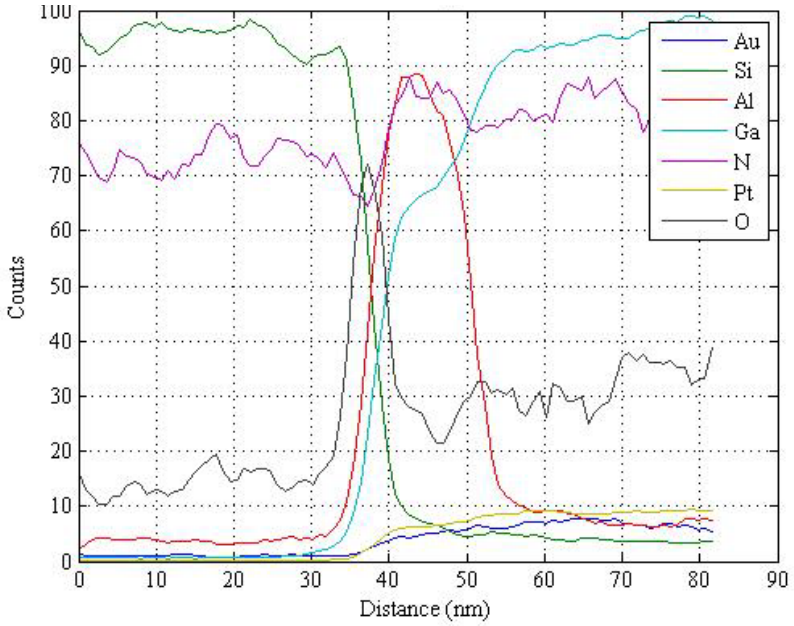

Figure 30. Line scan data from the fresh Pt Active layer line scan depicting the presence of each element analyzed.

Overall we noticed in the Pt samples, the general shape of the device was as expected. There were no large areas of visible dislocations or strained areas near the GaN/(Al, Ga)N layers. The oxygen presence was unexpected and we did not expect to see the foot or the dip area. We also expected to see a thin GaN cap in which this HEMT was built on to protect from diffusion. Since there was an absence of a Ga peak shown in Figure 27 and Figure 30 before the Al elemental line, it is likely that the GaN cap is not present after Pt device fabrication.

2. Degraded

The degraded Pt sample was electronically stressed at 1mA and -140V across the gate to source. The stressing parameters were held constant among all devices such that the gate to source voltage would be less than 0V. The stepping of V_{GS} would be -1V per 10 seconds and the drain to source voltage would be set equal to 0V.

The degraded device sample area was chosen from the electroluminescence information shown in Figure 31. The lighted areas show where there is a higher electroluminescence and therefore a higher probability of finding a defective region along

the gate. The electroluminescence areas were all along the source side of the gate, which is also physically closer to the gate than it is to the drain. We chose to make the sample around the 56.56µm point. This point had high intensity but was very concentrated in a small area. Neugebauer in [18] discusses the correlation between electroluminescence and dislocations in GaN. Note, the areas of higher electroluminescence are only present on the source side of the gate forming the main reason why we focused the imaging to this side of the gate in sample preparation in Chapter III.

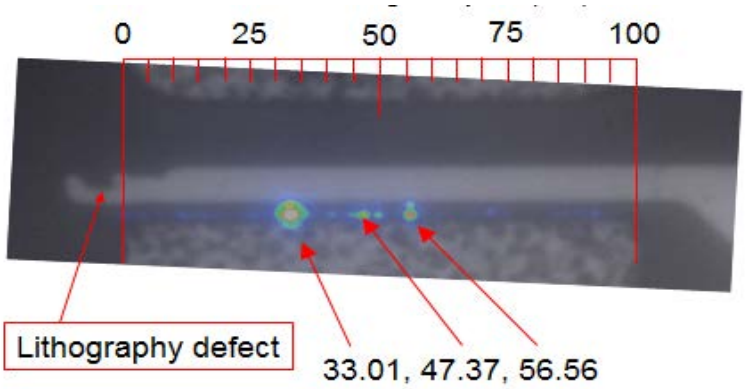

Figure 31. Electroluminescence intensity on degraded Pt gate. The arrows correspond to the distance across the gate in µm beginning at the edge of the source indicating areas of higher intensity.

Oxygen presence where we expected (Al, Ga)N to be is shown in Figure 32. There is a foot clearly visible in the red Au image and circled in blue. The (Al, Ga)N layer is clearly thinned in the Al image due to the lessening color intensity in the center of the image.

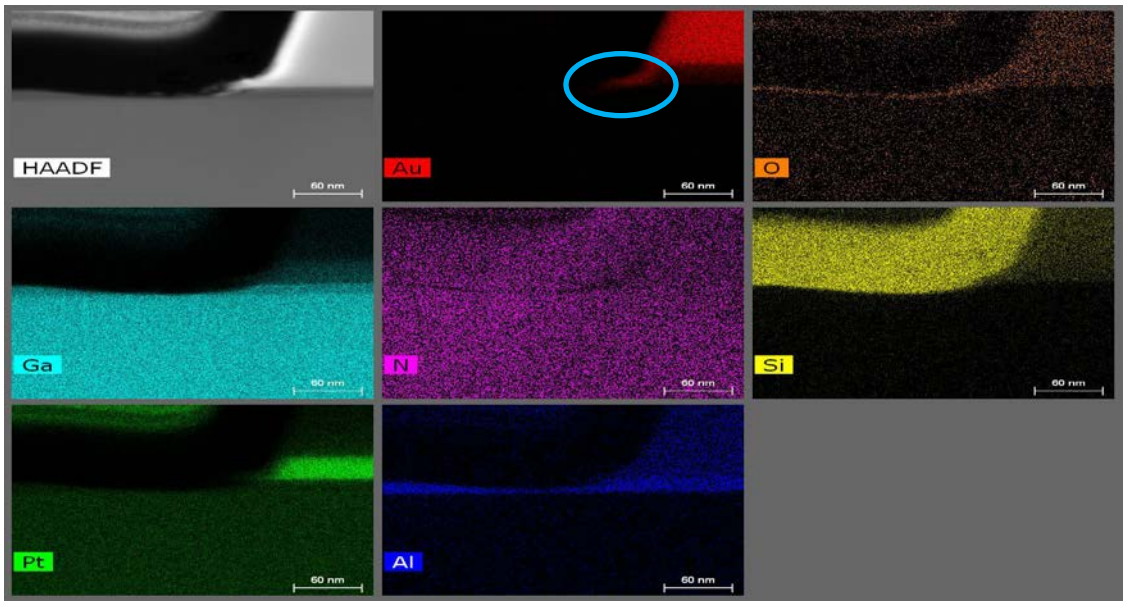

Figure 32. Elemental scans from the EDS for the degraded Pt device. The top left image is the HAADF followed by the seven singular elemental pictures (Au, O, Ga, N, Si, Pt, and Al).

The spectrum data shown in Figure 33 from the degraded Pt sample is similar that observed for the fresh sample in the elemental spectrum. The peak numbers for Ga are slightly less than those observed for the fresh sample spectrum, which could be due to potential differences in image scanning time. We tried to keep the scanning time to approximately 300s for all samples.

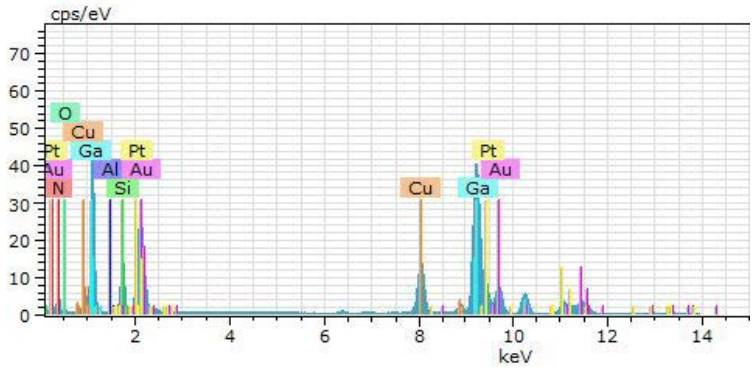

Figure 33. Elemental spectrum display of electron volts versus photon counts of the degraded Pt sample. The peaks in the spectrum correspond to individual elements present in imaged area.

The Au and Pt gate layer results shown in Figure 34 might appear to have a slight amount of oxygen present due to the higher oxygen levels until 40nm but the scan line is noisy leading most likely to a smaller concentration. However, there is not a peak of AlO_x present because the oxygen data drops significantly right as the Al line is increasing. The (Al, Ga)N and GaN layers appear to be free of diffusion due to the smooth Al and Ga lines and the drop off of other elements in the presence of those layers. The Si line was adjusted to be normalized to 10 to keep the graph's color scheme consistence with that used in other similar figures as Si was not actually present in this location of the scan.

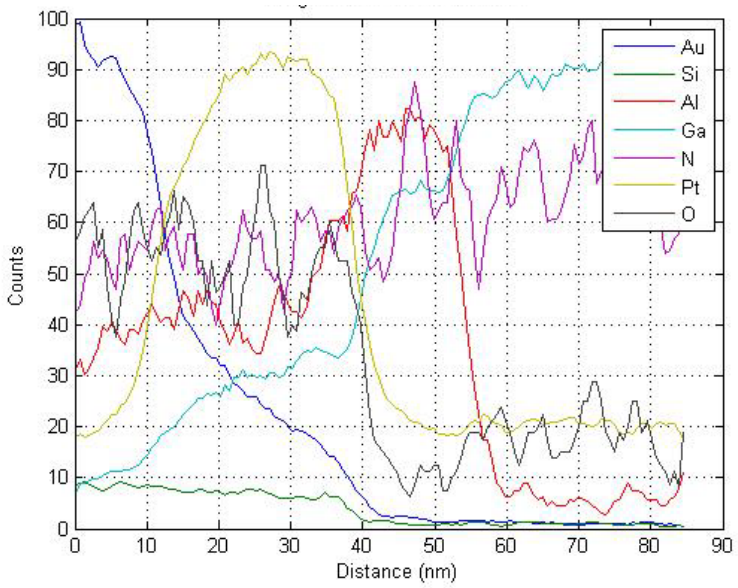

Figure 34. Line scan data of the degraded Pt gate line scan depicting the presence of each element analyzed.

Line scan data results obtained for the degraded and fresh Pt foot line scan, shown respectively in Figure 35 and 28 have differences worth noting. While the Si_3N_4 and GaN layers appear clear of diffusion, there is a peak of Au followed by a peak of Pt representing the foot seen in the HAADF image in Figure 32. The high and relatively smooth oxygen curve seem to show that this is not an artifact but instead corresponds to the formation of an AlO_x region before the (Al, Ga)N layer. The Pt line can only be read accurately until approximately 40nm due to the close x-ray diffraction between Ga and

Pt. The large peak of Ga in the spectral data shown in Figure 33 is causing the Pt to mirror Ga from 40nm onward as shown in Figure 35.

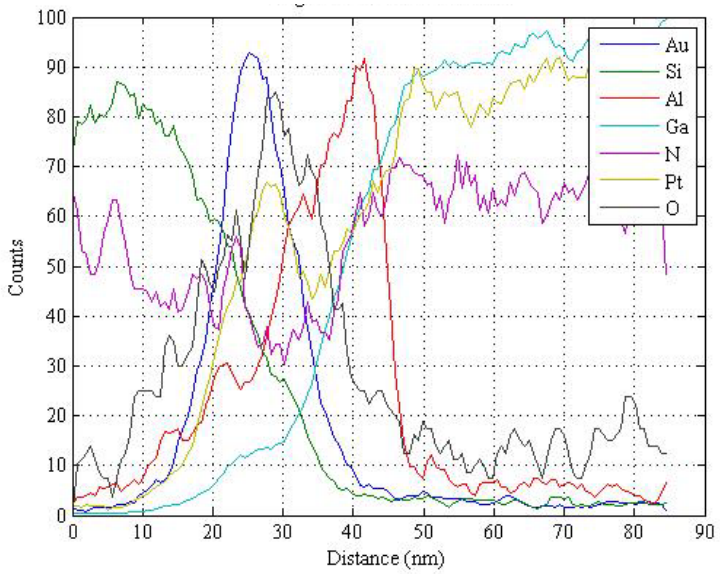

Figure 35. Line scan data of the degraded Pt foot line scan depicting the presence of each element analyzed.

The dip area remains thin. There is no presence of Pt spiking in the dip. However, Figure 36 shows a spike in Au in the dip opposed to the Au. AlO_x took the place of the (Al, Ga)N layer but the GaN layers appear unaffected. The dip area is composed of Au, Al and oxygen. In the plot Pt element was modified to have a count maximum of 10 percent the original data because it did not have a significant contribution.

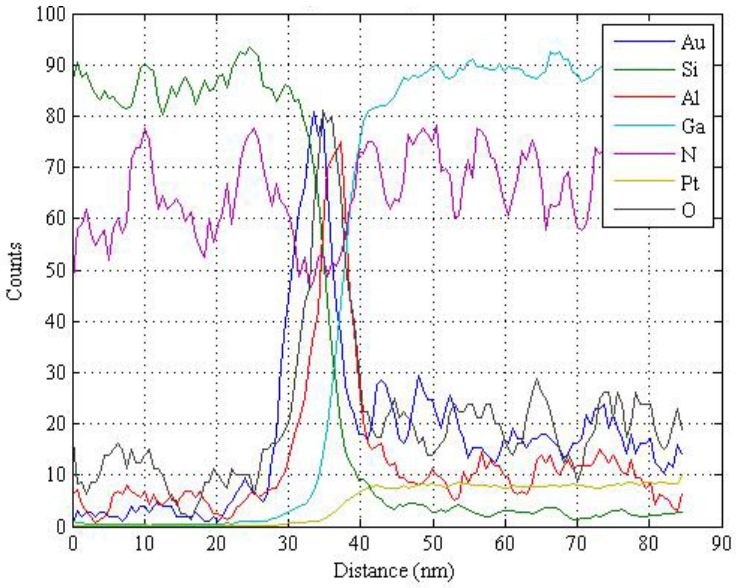

Figure 36. Line scan data from the degraded Pt dip line scan depicting the presence of each element analyzed.

The active layer is relatively clear of any noticeable diffusion as shown in Figure 37. The oxygen peak remains present between Si_3N_4 and (Al, Ga)N layers. Both Au and Pt plots were adjusted to have their count maximum scaled to 10 vice 100 to minimize their visual effect on the overall plot.

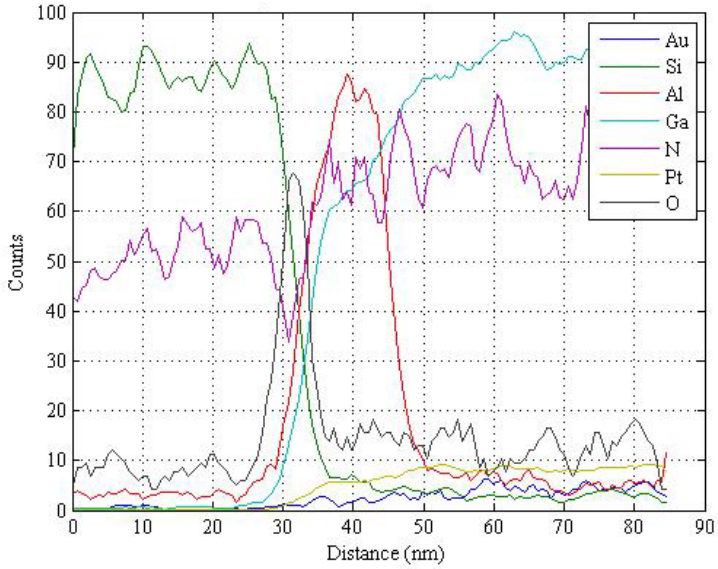

Figure 37. Line scan data of the degraded Pt active layer line scan depicting the presence of each element analyzed.

3. Failed

The failed Pt device was electrically stressed under the same stepping parameters as the degraded Pt device but instead of having an amperage across the gate equal to 1mA and a V_{GD}=-140V. In the failed device, the amperage increased until the device reached a breakdown as depicted in Figure 38.

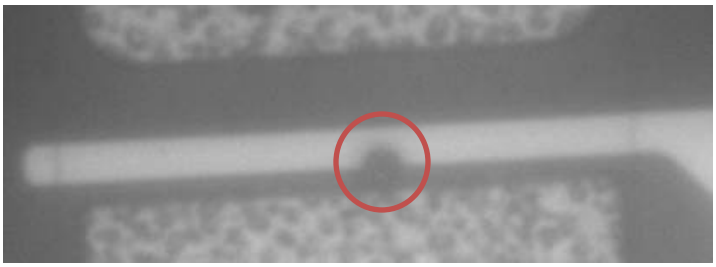

Figure 38. SEM image from NRL of failed Pt device after catastrophic failure. The breakdown area is circled in red.

The failed device was the first device we made using the procedure in Chapter III. We wanted to remove the area around where the visible defect was in Figure 38 in order to see which elements were present in the catastrophic failure area. We chose our sample location to be centered on the large hole created in the gate of the device shown in Figure 38. This device was then used as a baseline for the sample preparation and analysis of subsequent stressed devices.

The cross section of the device in Figure 39 demonstrates why the lift out sample preparation method is preferred. Other methods would not be structurally sound to survive multiple machine processes. The red oval in Figure 39 shows the hole preserved in the sample.

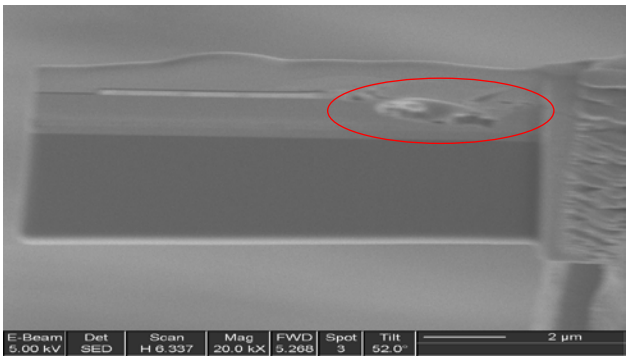

Figure 39. SEM image of failed Pt device sample with large defect circled in red.

This hole shown in Figure 39 shows a major degradation. The degradation goes all the way down into the GaN layer and almost into the silicon substrate. We thinned this sample and examined the hole in the Titan STEM. Figure 40 represents the composite of four higher resolution areas imaged and analyzed in the Titan. The first image on the left shows where the gate ends. The gate should continue to the third image but the degradation was so severe that the gate was completely removed.

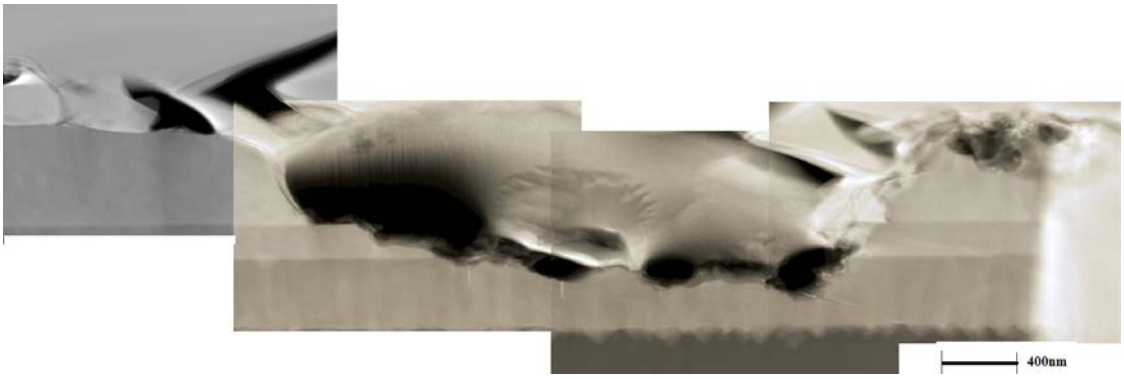

Figure 40. STEM composite image of the failed Pt device sample focused on the large defect area.

When we looked at the elemental composition of the failed region in Figure 41, we saw that the oxygen (orange image) concentration appeared to outline each of the voided areas. We were also able to determine that gate appeared to break off as evident in the Au (red) image in Figure 41. The presence of oxygen in this image led us to consider

oxygen as a contributing factor for dislocations and reliability errors. However, because this area was so damaged we could not use it in drawing linear comparisons as to what occurred at the gate edge.

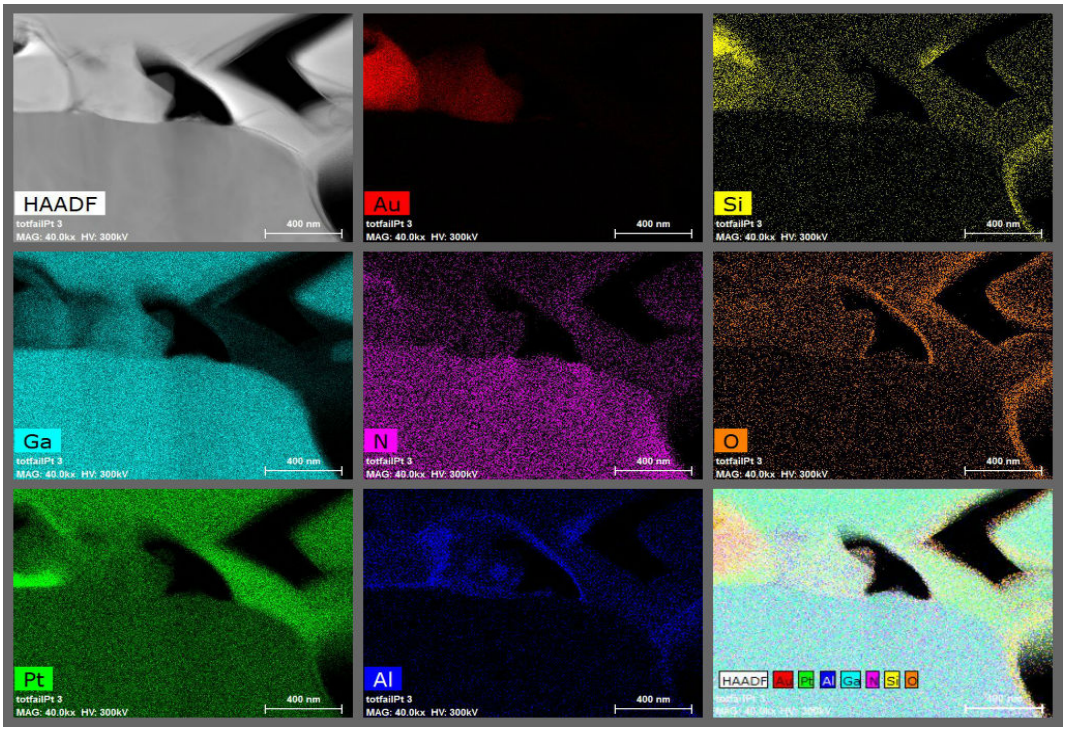

Figure 41. Elemental scans from the EDS for the failed Pt gate on the source side with major degradation of the gate edge. The first image is the HAADF followed by the seven singular elemental pictures (Au, O, Ga, N, Si, Pt, and Al).

We chose to look at the drain side of the gate edge once we saw confirmation of the presence of oxygen on the source side of the gate. The drain side of the gate was still intact as shown in Figure 39. The elemental breakdown of the failed drain side of the gate is shown in Figure 42. The dip and foot are both present in the source side.

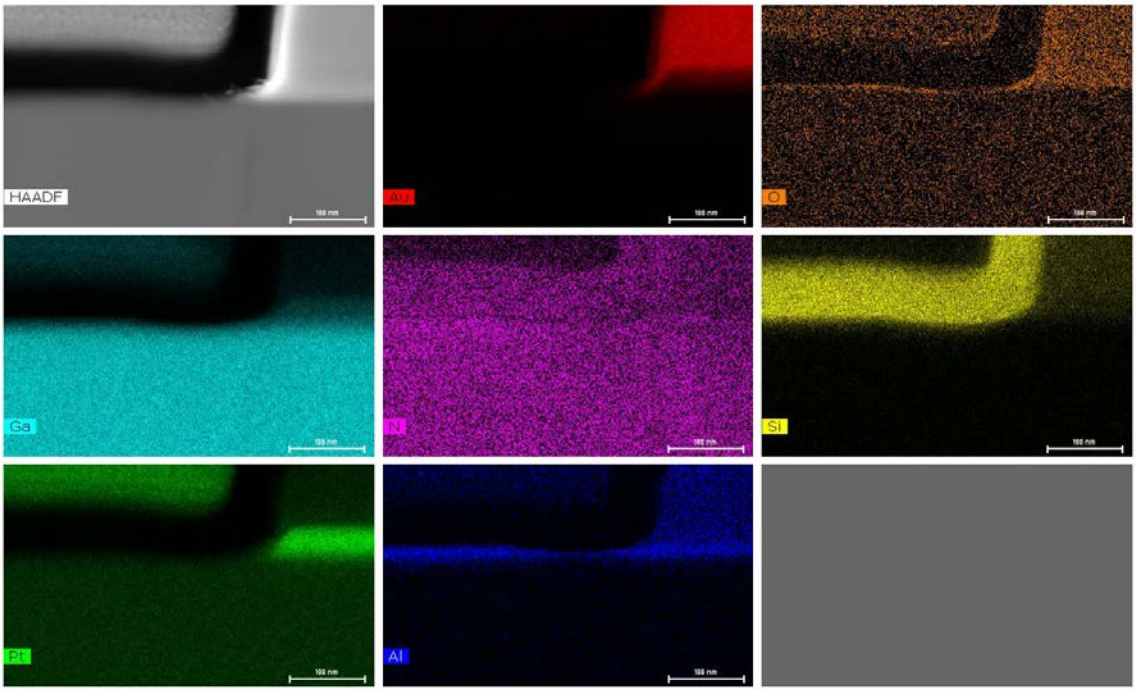

Figure 42. Elemental scans from the EDS for the failed Pt gated device. The first image is the HAADF followed by the seven singular elemental pictures (Au, O, Ga, N, Si, Pt, and Al).

The spectral data shown in Figure 43 is also similar to that observed for the drain side of the previous Pt samples. Thus we continued to use this spectral data as another guide due to the similarities in each side.

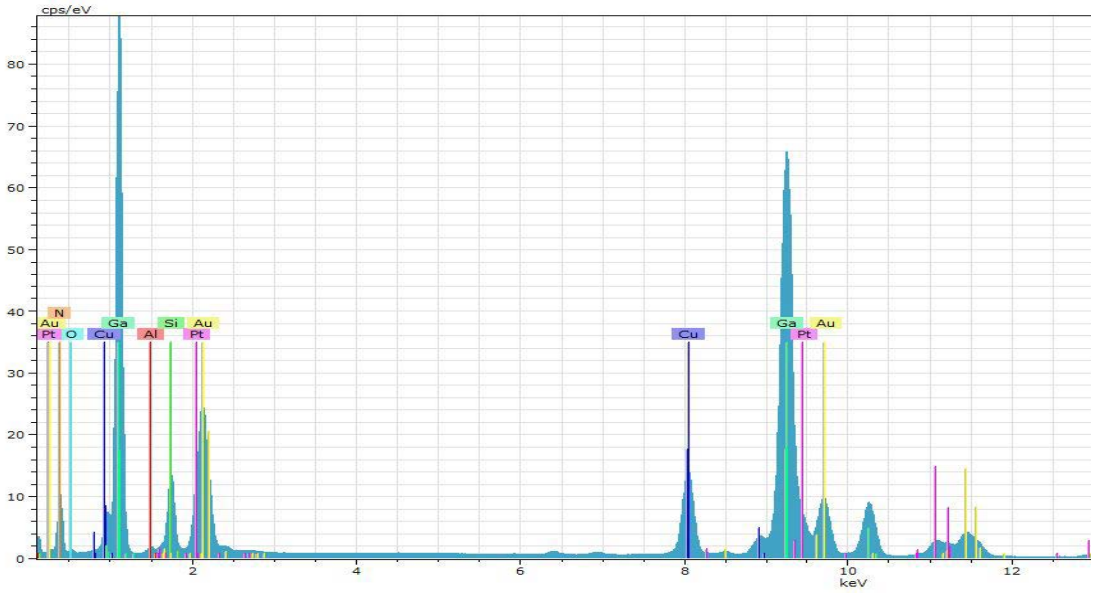

Figure 43. Elemental spectrum display of electron volts versus photon counts of the failed Pt sample. The peaks in the spectrum correspond to individual elements present in imaged area.

Similar to the previous Pt gate line scans, there is oxygen present in both the Au and the Pt gate. The oxygen diffuses into the (Al, Ga)N layer. The largest change to note from Figure 44 is the large diffusion distance the Pt has into the (Al, Ga)N layer. The Pt diffuses across the entire (Al, Ga)N layer and only stops once it hits the GaN layer. The Si data was minimized as it was not a relevant factor for this line scan. Similarly to the other device scans, there was no presence of a 2nm GaN cap.

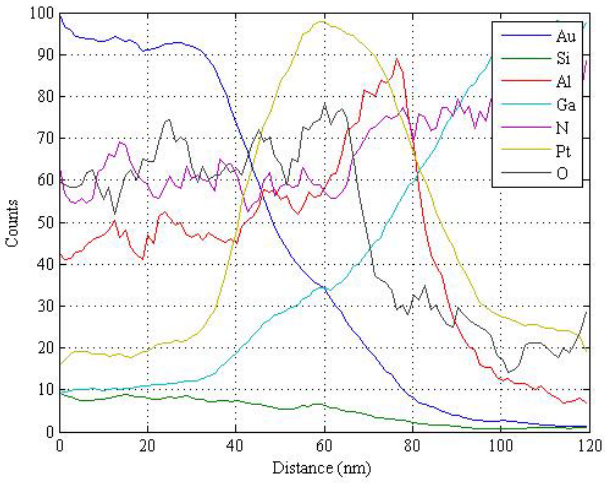

Figure 44. Line scan data for the failed Pt gate line scan depicting the presence of each element analyzed.

Continuing to the foot area of the sample in Figure 45, the Au and Pt are both present. The oxygen is also mostly present in the Au foot. The diffusion of the Pt into the (Al, Ga)N layer even at the foot. Looking at the Pt presence in the GaN layer and comparing it to the spectral data for this sample in Figure 42, the second Pt peak is mostly attached to the high Ga count and is therefore an artifact and should not be counted. The GaN layer remains clean as well.

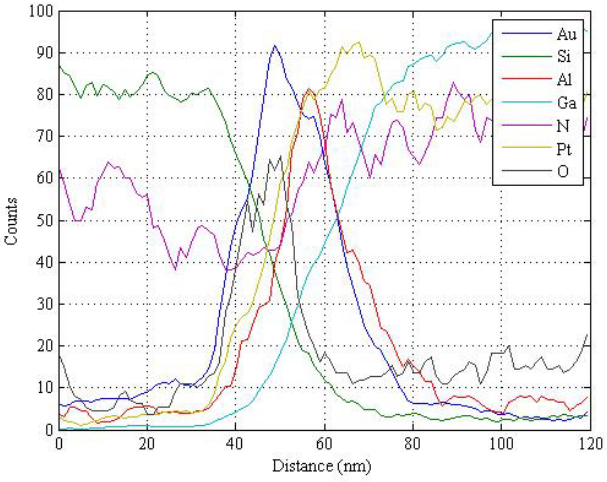

Figure 45. Line scan data of the failed Pt foot line scan depicting the presence of each element analyzed.

The dip area in Figure 46 has AlO_x before the thinned (Al, Ga)N layer. Au does not travel into the dip area. Note this is a difference from previous Pt fresh sample results but could be due to this being the drain side instead of the source side.

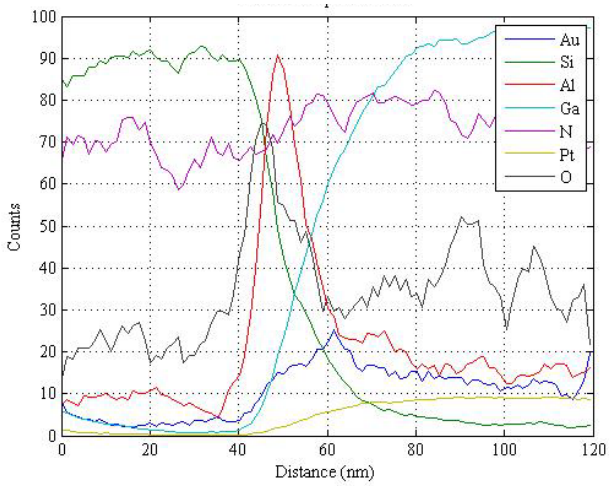

Figure 46. Line scan data of the failed Pt dip line scan depicting the presence of each element analyzed.

The active layer line scan in Figure 47 contains the same information as that shown in Figure 30 of the previous Pt active layer line scans. The lack of elemental changes across the active layer region is good because it narrows the areas of concern in finding defects within each device. The Pt and Au data were normalized after analysis of the raw line scan data to 10 vice 100 to keep colors consistent as they were not found to be a major contributing factor.

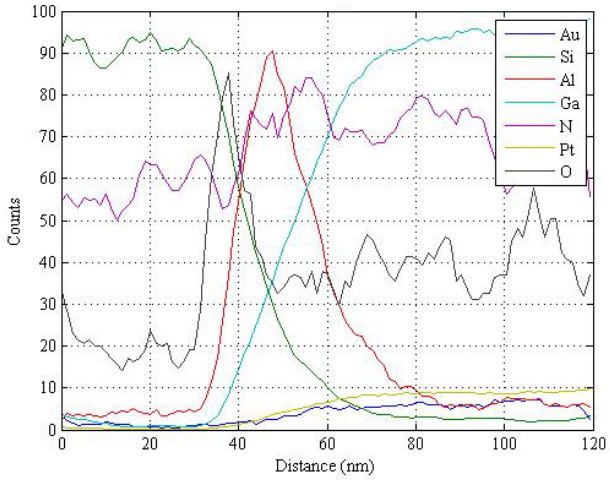

Figure 47. Line scan data of the failed Pt active layer line scan depicting the presence of each element analyzed.

C. NICKEL DEVICES

There were three Ni devices examined and analyzed for this sample set: fresh, degraded and failed. All three samples were analyzed in the same four locations as the Pt devices considered in Figure 23 to keep consistency. The Ni device samples were made after the Pt samples using the sample preparation procedures described in Chapter III. Any major visible area of degradation was avoided for sample extraction and efforts were made to focus on areas of high electroluminescence intensity. We examined the source side of these devices.

1. Fresh

Similarly to the Pt fresh device, the fresh Ni device did not undergo any electrical stressing and was used for identifying any processing discrepancies and the baseline for trends within the stressed devices. There is a "foot" present along the gate edge shown in Figure 48 circled in blue and is similar to the Pt samples. There is also a "dip" area circled in red for the Ni devices; however, it appears to be less deep than in the Pt samples. Note that the Pt element image has been replaced with the Ni image. There is still Pt present serving as the protective cap above the Si_3N_4 layer but this area was not evaluated in the line scans and was omitted.

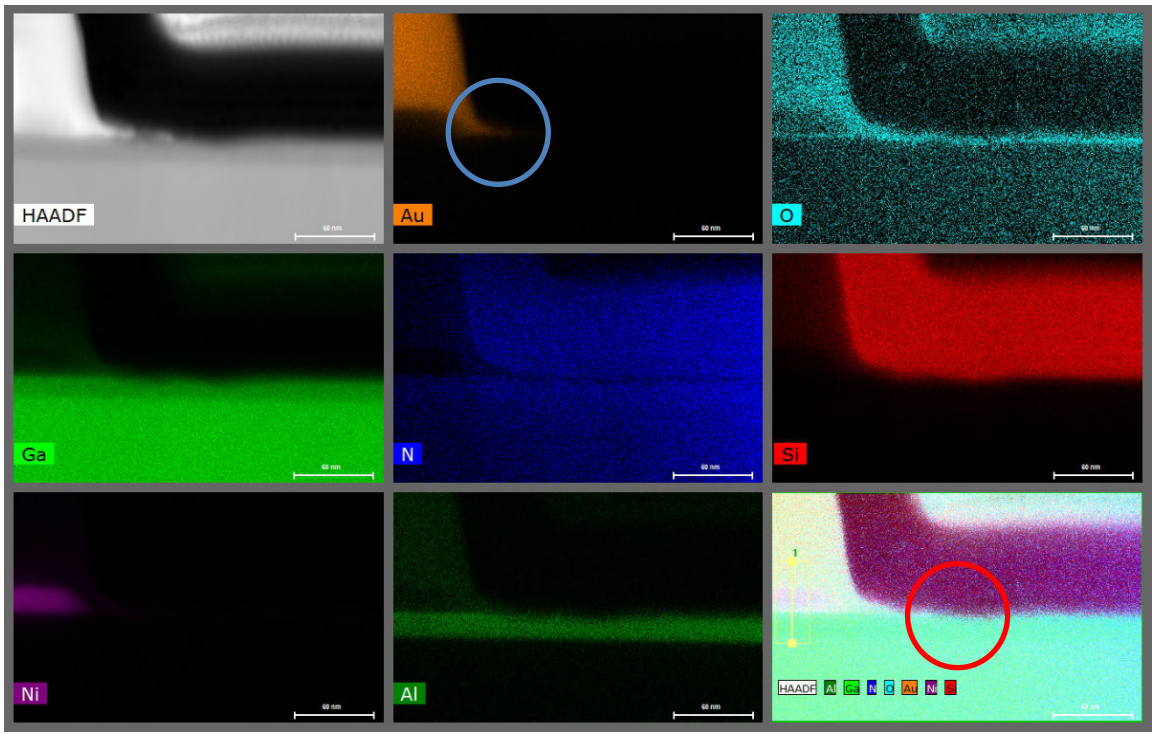

Figure 48. Elemental scans from the EDS for the fresh Ni gated device. The First image is the HAADF followed by the seven singular elemental pictures (Au, O, Ga, N, Si, Ni, and Al), ending with the composite picture of those seven elements.

The spectral data seen in Figure 49 is slightly different than that obtained with the Pt devices as it has the added element of Ni. The number of photon counts is also similar to the previous samples due to ta consistent 300 second exposure time ensuring consistent comparisons.

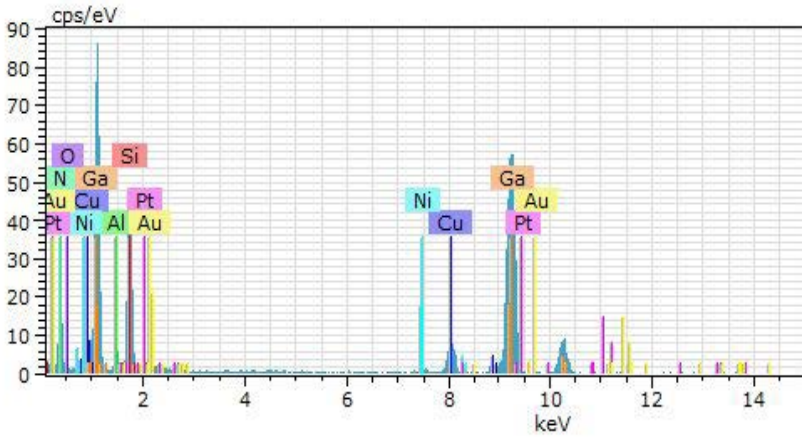

Figure 49. Elemental spectrum display of electron volts versus photon counts of the fresh Ni sample. The peaks in the spectrum correspond to individual elements present in imaged area.

The fresh Ni device had very smooth lines as shown in Figure 50. The Au layer was found to have a higher presence of oxygen than the Ni area. The oxygen line did peak when it came into contact with the Al, thus creating a thin layer of AlO_x between the nickel and the (Al, Ga)N layers. The presence of the AlO_x in a fresh device under the gate is concerning as this AlO_x was not expected under the gate due to the fabrication process of the device and substrate. The 2nm GaN cap should provide protection but is not present in the line scan of any of the fresh devices.

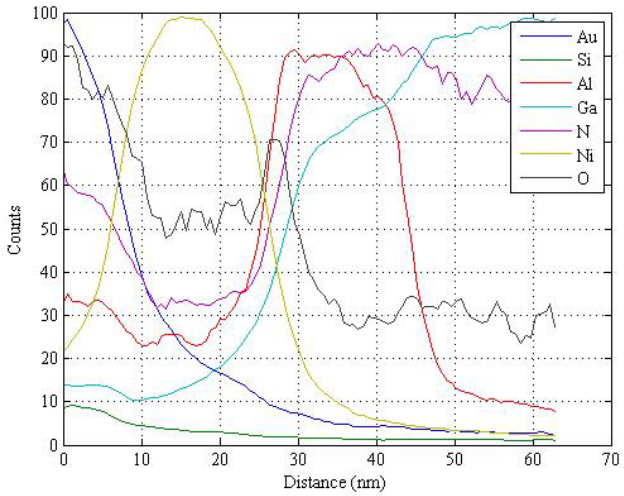

Figure 50. Line scan data for the fresh Ni gate line scan depicting the presence of each element analyzed.

The foot area shown in Figure 48 is less prominent than that indicated in the Pt fresh device shown in Figure 25. The line scan data shown in Figure 51 along with the high intensity of the Si and Ga elemental images indicate clear Si_3N_4 and GaN layers. The "foot" area is composed of nickel and Au. The oxygen that was present under the gate still appears in the foot, but as well as spikes after the foot before the (Al, Ga)N layer indicating that the AlO_x is still present under the foot.

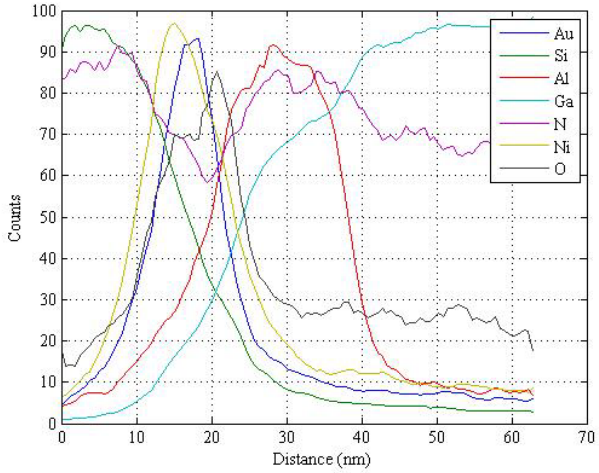

Figure 51. Line scan data for the fresh Ni foot line scan depicting the presence of each element analyzed.

Results shown in Figure 52 indicate the Si_3N_4 and GaN layers are clear and definitive. The Ni does travel into the dip where the Au is not present. The oxygen line also follows the nickel almost identically but the Al line increases before the Ga and N lines showing that the AlO_x layer is still present.

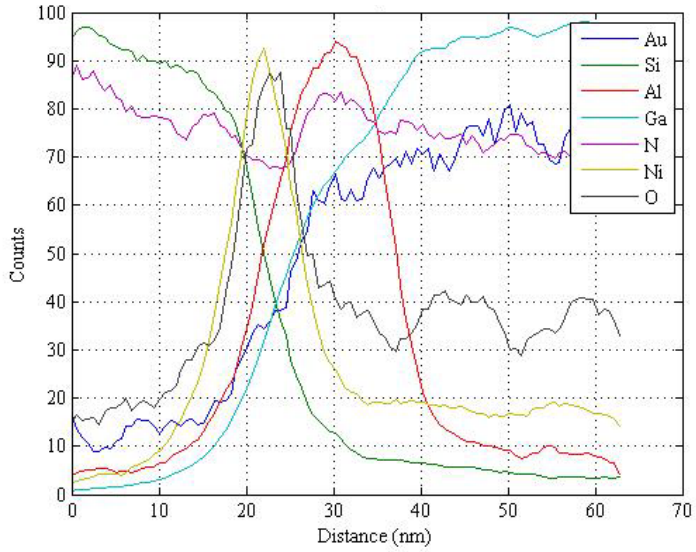

Figure 52. Line scan data of the fresh Ni dip line scan depicting the presence of each element analyzed.

Line scan data plotted in Figure 53 indicate the clear presence of Si_3N_4 and GaN layers. In addition, results show the presence of AlO_x above the (Al, Ga)N layer but no GaN cap above the (Al, Ga)N layer.

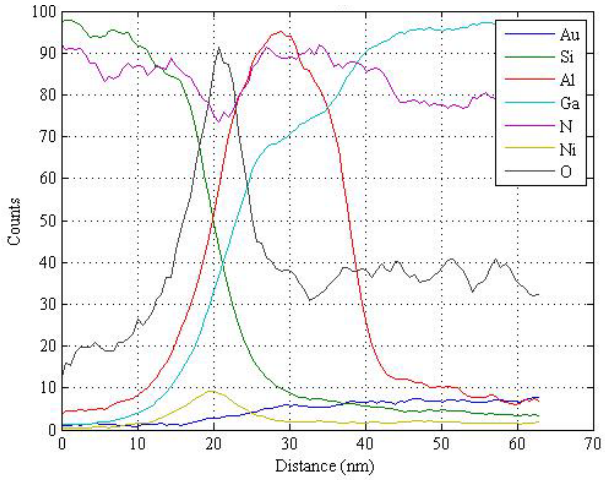

Figure 53. Line scan data of the fresh Ni active layer line scan depicting the presence of each element analyzed.

2. Degraded

The degraded Ni device was electrically stressed using the stepping method shown in Figure 4 to a V_{GD}=-130V and a gate current I_G=1mA. The gate current parameter remained the same in both the Ni and the Pt degraded devices but gate to drain voltage differed by 10V. The electroluminescence image in Figure 54 contains the areas of high electroluminescence near the source edge of the gate, thus inferring the highest probability for defects. The degraded sample was obtained from cutting the section shown at the 34.54µm distance because it was a small but highly concentrated electroluminescent area.

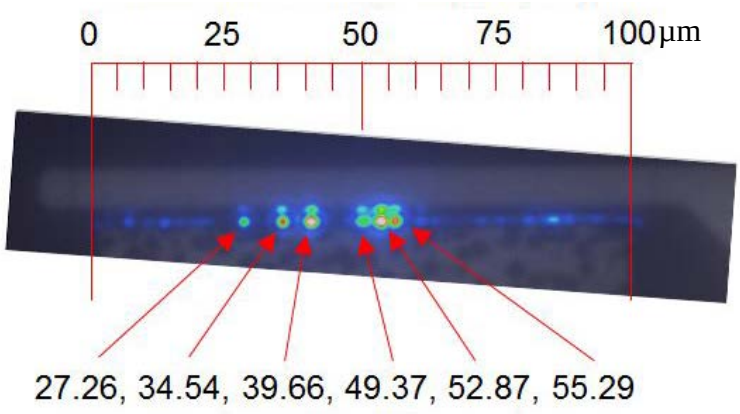

Figure 54. Electroluminescence after stressing on the degraded Ni gated HEMT. The arrows correspond to the distance across the gate in µm beginning at the edge of the source indicating areas of higher intensity.

The degradation in this area was not catastrophic enough to leave a hole or any large visual damage. The intention behind choosing the 34.54µm area was to have a cross section of a device that had undergone the electrical stressing but had not degraded so much as to noticeably change the structure as with the failed Pt device considered in Figure 38.

The elemental analysis of the gate edge is shown in Figure 55. The “foot” area along the gate edge does not extend as far as the Pt device. The dip area is less noticeable upon visual inspection. The Al elemental image shown in Figure 55 captures the smaller

dip area very clearly. We expect to see a larger (Al, Ga)N layer in comparison to the Pt devices due to the dip region begin smaller in the Ni devices.

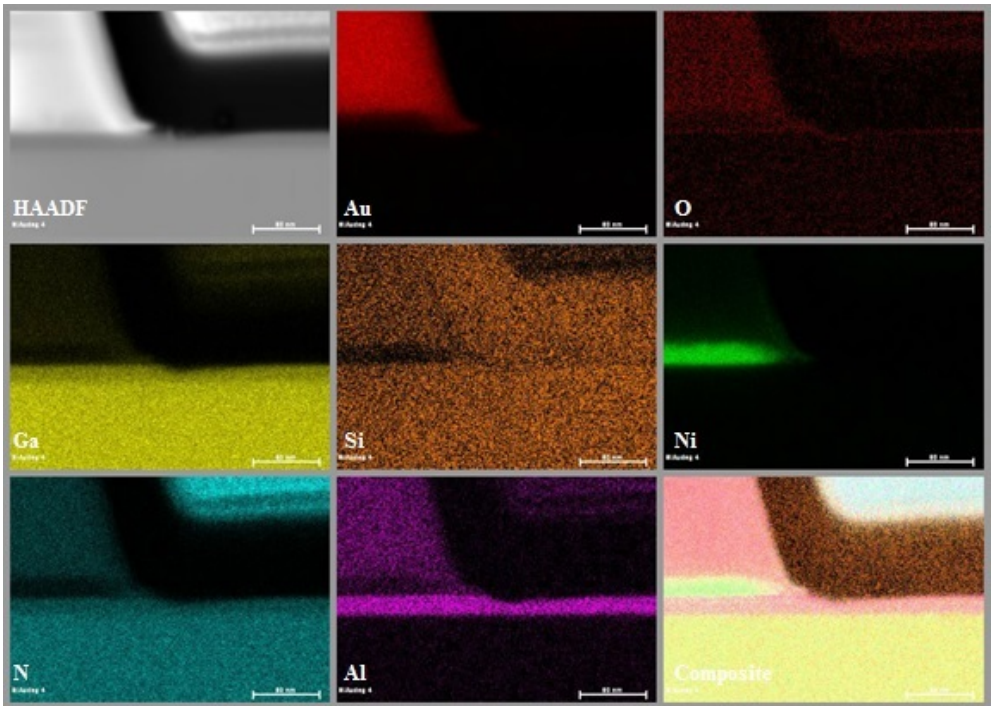

Figure 55. Elemental scans from the EDS for the degraded Ni gated device. The first image is the HAADF followed by the seven singular elemental pictures (Au, O, Ga, Si, Ni, N and Al), ending with the composite picture of those seven elements.

The spectral data plotted in Figure 56 is similar to that obtained for the Ni fresh device. This finding is expected because the device type is the same; however the peak heights are not as high as those shown for the fresh Ni gated device. This lower height along the y-axis for photon counts is due to this image only being imaged for approximately 200 seconds vice the 300 seconds taken in other scans.

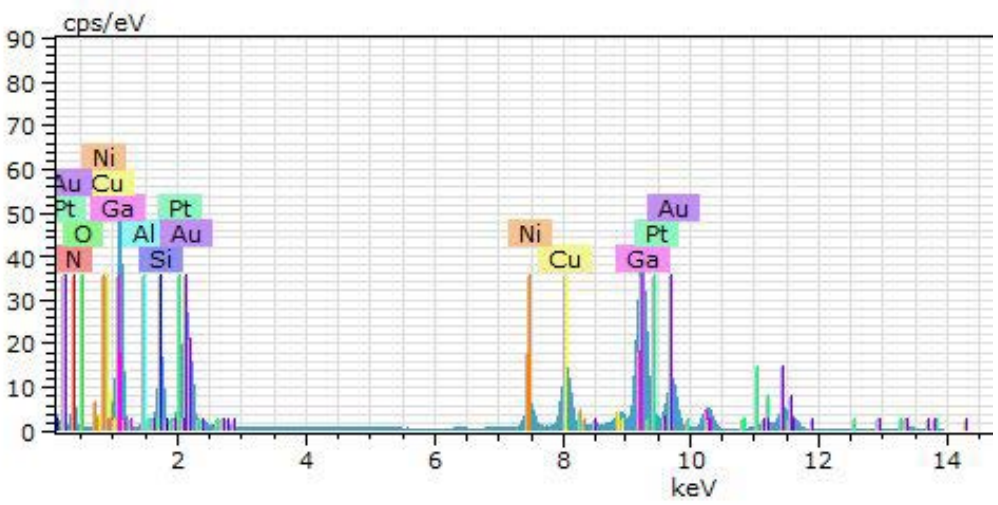

Figure 56. Elemental spectrum display of electron volts versus photon counts of the degraded Ni sample. The peaks in the spectrum correspond to individual elements present in imaged area.

The degraded gate line scan in Figure 57 begins with in the metal gate region. There is oxygen present in the Au layer but not in the Ni layer of the gate metal. There is a slight increase where the aluminum line rises indicating that there is most likely AlO_x present before the (Al, Ga)N layer. The GaN layer remains clear due to the high intensity of the Ga image in Figure 55 and the smooth line in the GaN region shown in Figure 57.

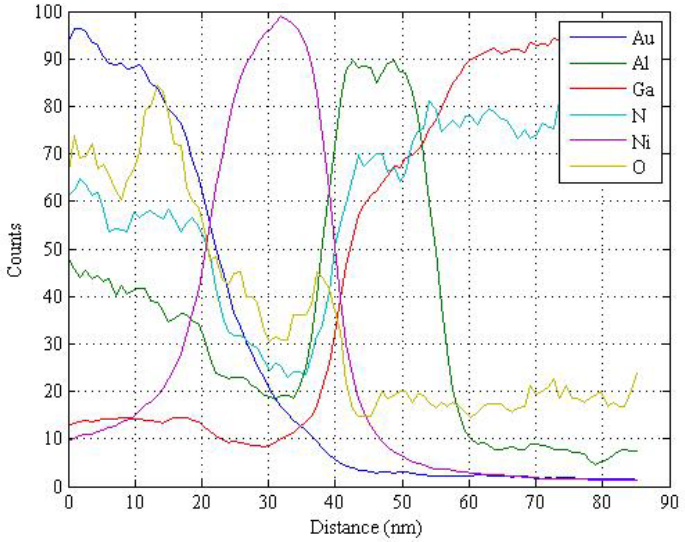

Figure 57. Line scan data of the degraded Ni gate line scan depicting the presence of each element analyzed.

The foot area in Figure 58 has clean Si_3N_4 and GaN layers. The foot is composed of the gate metals Au and Ni shown by the double peak of Au and Ni around the 30–40nm distance in Figure 58. The (Al, Ga)N layer also is free and clear of an AlO_x layer because the oxygen peak is only within the Ni and Au region.

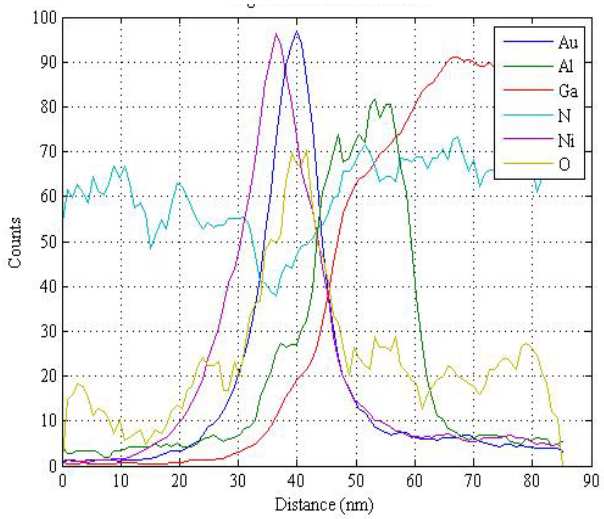

Figure 58. Line scan data of the degraded Ni foot line scan depicting the presence of each element analyzed.

The dip area line scan in Figure 59 contains a definitive AlO_x layer between the Au and the (Al, Ga)N shown at the 40nm distance. The Si_3N_4 and GaN layers remain clear. Au is still present in the dip area but the noise level in the Ni line leads us to conclude that Ni does not travel all the way into the dip area and can be considered an artifact.

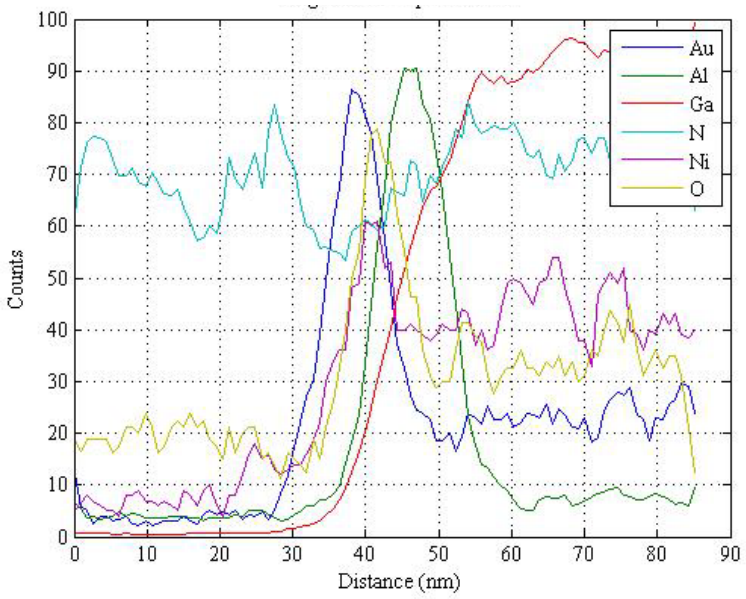

Figure 59. Line scan data of the degraded Ni dip line scan depicting the presence of each element analyzed.

Investigating the active layer approximately 100nm from the gate edge, we see very clear lines for the Si_3N_4, AlGaN and GaN layers suggesting these areas are not affected by diffusion of other chemical elements. However, oxygen is present and shown in Figure 60 at the 30nm distance. The oxygen peak rises at the same distance as the aluminum creating an AlO_x layer before the (Al, Ga)N layer.

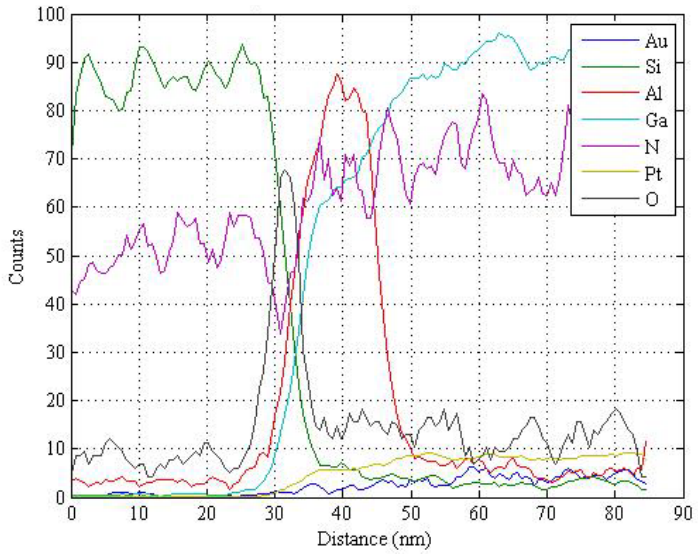

Figure 60. Line scan data of the degraded Ni active layer line scan depicting the presence of each element analyzed.

The AlO_x layer is present throughout the entire gate edge area in Figure 48 with the exception of the dip area. The Si_3N_4 and GaN layers remained unchanged throughout the entire area. The Ni within the gate showed a slight amount of diffusion into the AlGaN layer.

3. Failed

The failed Ni gated device was the last device to be analyzed. The device was electrically stressed to the point of failure using the stepping procedure shown in Figure 4. The electroluminescence is highlighted across the source sided gate edge of the entire device shown in Figure 61. We wanted to examine an area along the gate that did not have a visual defect so that we could examine the elemental composition of the point of breakdown. Thus, we chose to take our sample from the 17.84µm location, as the 1.53µm area after the stressing contained a visual defect.

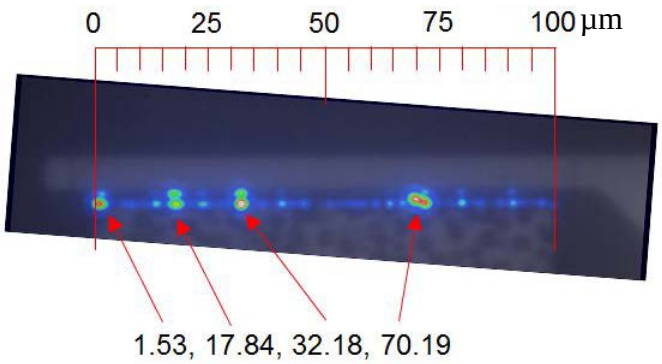

Figure 61. Electroluminescence after stressing on the failed Nickel gated HEMT. The arrows correspond to the distance across the gate in µm beginning at the edge of the source indicating areas of higher intensity.

The sample was scanned for 300 seconds. The elemental scans of the failed device shown in Figure 62 have a foot and dip area. However, the foot and the dip in the Au and Al image look slightly different from those shown in previous scans. Here, the foot does not seem as prominent and the dip does not seem as clear cut but rather has a lighter less intense Al area circled in red. The Ni image shown in Figure 62 does not slide or move into the dip at all. The spectral data shown in Figure 63 is similar in the photon counts to some found in the previous samples.

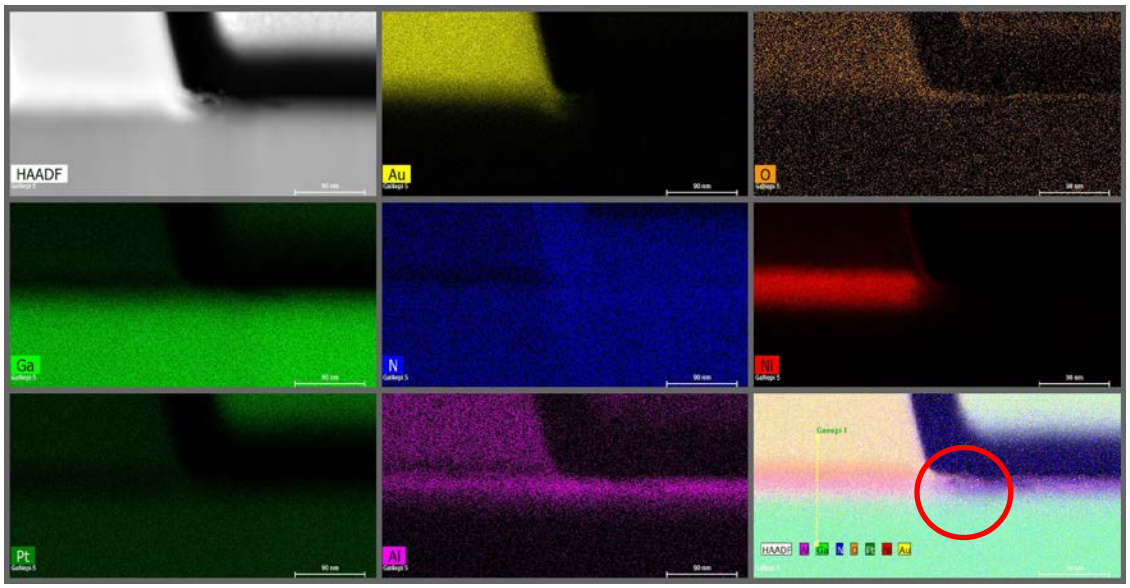

Figure 62. Elemental scans from the EDS for the failed Nickel gated device. The top left image is the HAADF followed by the seven singular elemental pictures (Au, O, Ga, N, Ni, Pt, and Al), ending with the composite picture of those seven elements.

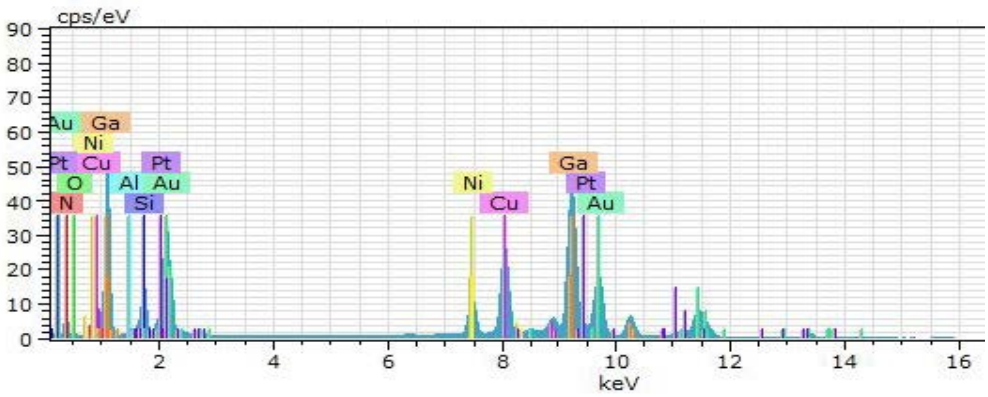

Figure 63. Elemental spectrum display of electron volts versus photon counts of the failed Ni sample. The peaks in the spectrum correspond to individual elements present in imaged area.

The gate line scans shown in Figure 64 are the most interesting. The oxygen is present only in the Au layer but not in the Ni layer of the gate. Ni does diffuse entirely into the (Al, Ga)N layer but stops once the GaN layer begins, as seen in the 30–70nm

distance. While oxygen was present in the fresh and degraded Ni samples, the (Al, Ga)N layer of the failed Ni sample does not contain oxygen as there is no strong peak of oxygen in the entire sample.

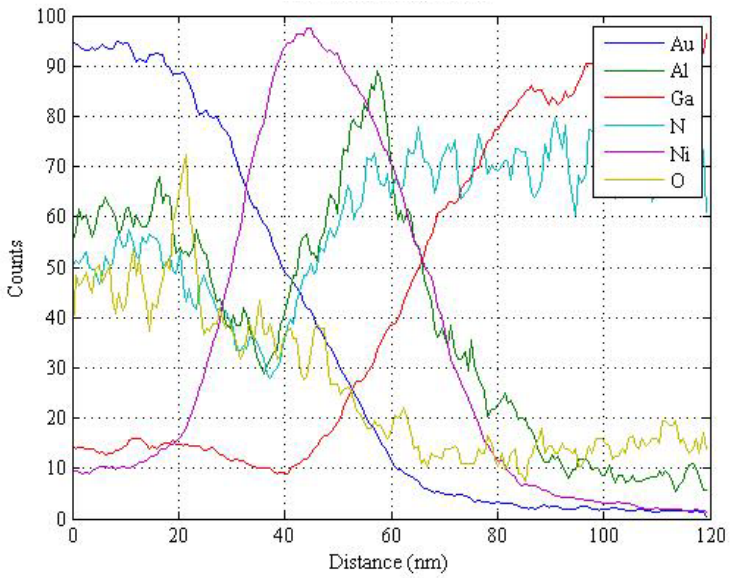

Figure 64. Line scan data for failed Ni gate line scan depicting the presence of each element analyzed.

The foot area line scan shown in Figure 65 indicates the presence of a clear Si_3N_4 layer and a GaN layer. The foot is composed of both Au and Ni. The oxygen that was present in the Au area is still present in this failed sample at the 45nm distance. The Ni diffusion is still present in the foot and extends through the (Al, Ga)N layer up to the GaN layer.

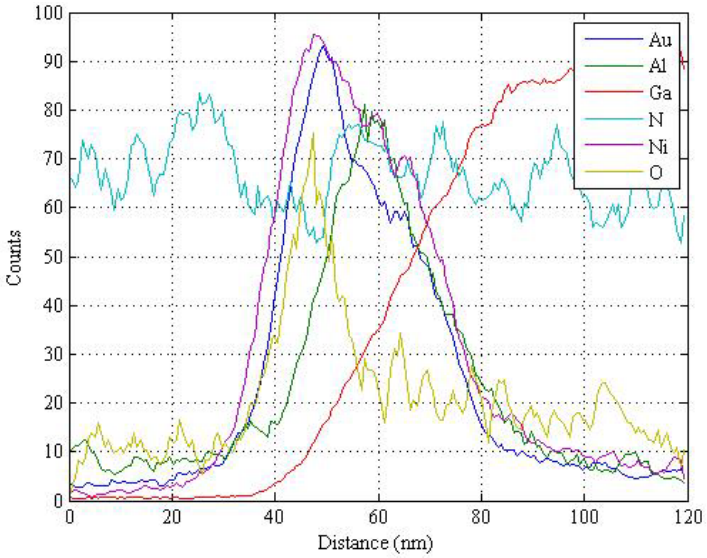

Figure 65. Line scan data of the failed Ni foot line scan depicting the presence of each element analyzed.

The "dip" line scan, shown in Figure 66, does not contain Au or Ni; this was also confirmed in the EDS elemental pictures. Once again, the Si_3N_4 and the GaN layers remain unaffected. The AlO_x layer is present before the (Al, Ga)N layer as the oxygen concentration begins to rise along with the Al concentration at the 30nm distance and peaks at 40nm.

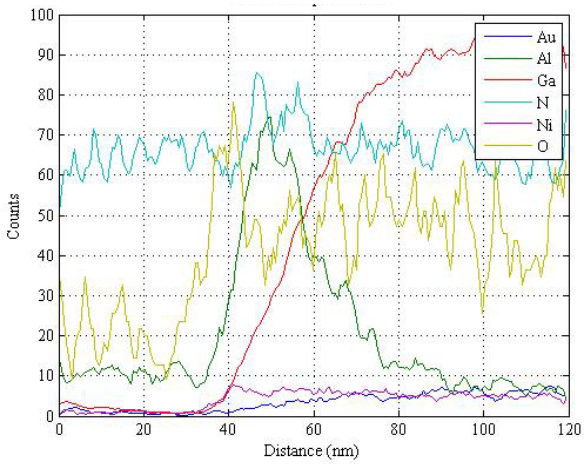

Figure 66. Line scan data for the failed Ni dip line scan depicting the presence of each element analyzed.

The active layer line scan in Figure 67 has clean Si_3N_4 and GaN layers. The AlO_x layer is also present. The rise in oxygen and Al concentrations occurs together at the 35nm distance. There is no Au or Ni present in the active layer scan.

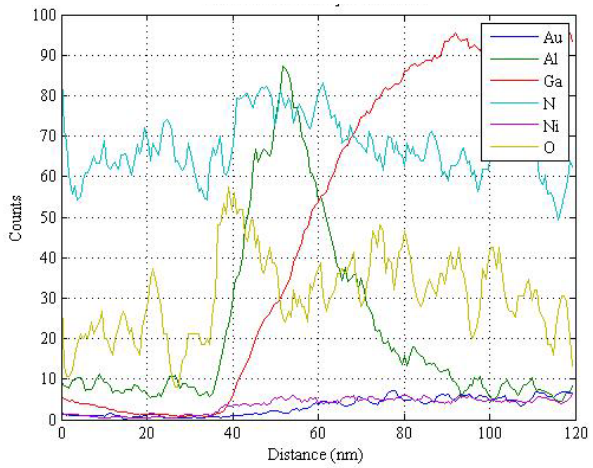

Figure 67. The line scan data for the failed Ni active layer line scan depicting the presence of each element analyzed.

D. COMPARISONS

We compared all seven devices against each other in our analysis of the line scans. Figure 68 highlights the presence of O under the gate of the fresh Pt gated device. We saw the presence of O and most likely AlO_x at the gate metal/(Al, Ga)N interface in every device.

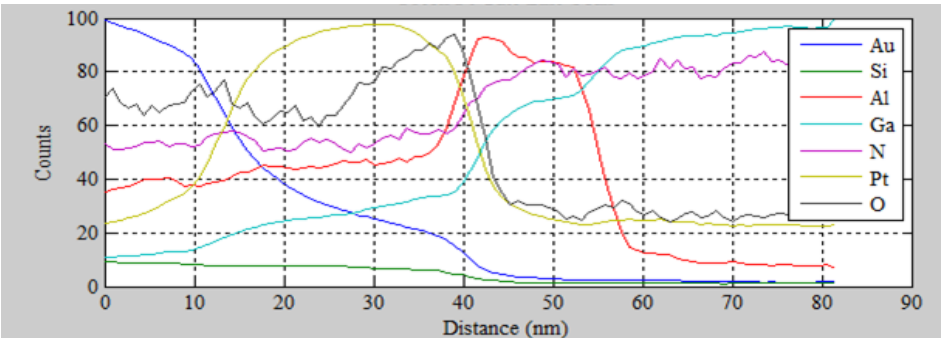

Figure 68. Fresh Pt gate line scan data.

We failed to see an expected GaN cap on both fresh devices. We expanded our original sample set of six to seven in order to rule out the possibility that the Nitronex, Inc© epitaxial layer was missing it or that the EDS detector was not capable of reading it. As seen in the highlighted area of Figure 69, the slight peak in the GaN area at approximately 5nm, does confirm the presence of the GaN cap as well as the detector's abilities.

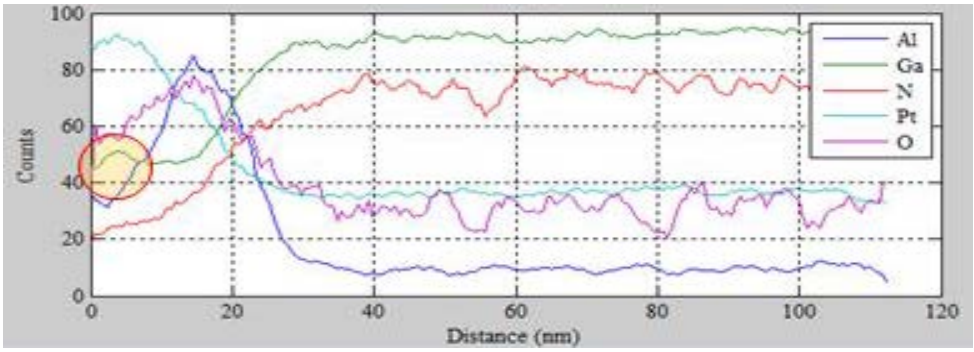

Figure 69. Epitaxial line scan with GaN cap present in highlighted area.

As seen in Figure 70, two Ni gates are compared at the gate line scan. The stressed Ni diffuses entirely through the (Al, Ga)N layer but stops when the Al disappears. This phenomenon is also present in the Pt gated devices. The diffusion of the gate metal occurred not only on the Pt gate but the trend was noticed on the opposite side of the gate at the drain edge leading to conclude that the entire gate width is experiencing this diffusion and it is not localized to only the source side.

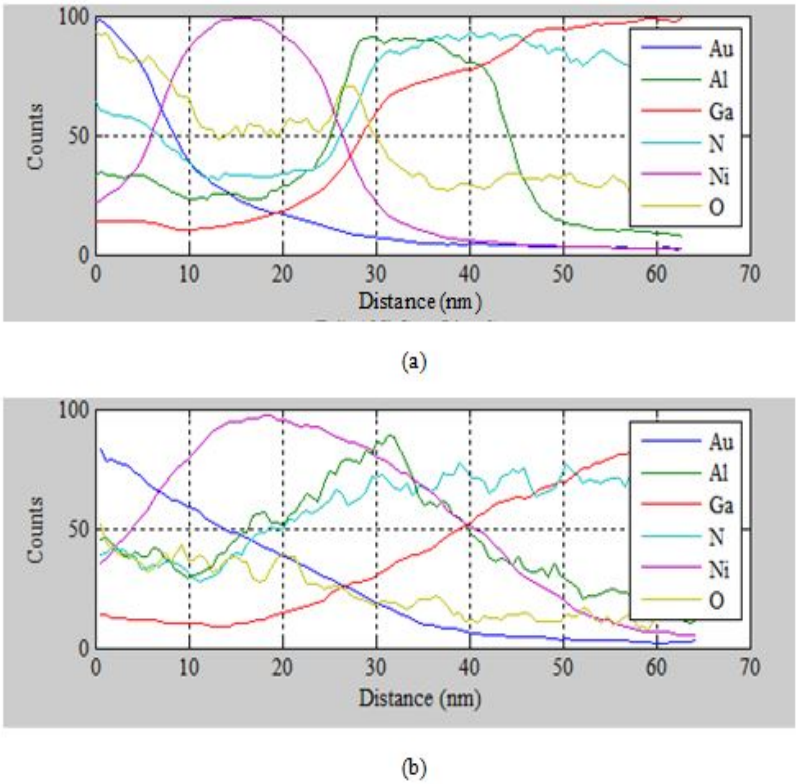

Figure 70. Fresh (a) and failed (b) Ni gate line scan data depicting the change in the location of Ni in the same region of both devices.

Line scans from the seven samples were analyzed and certain chemical trends were ascertained. The trends found were identified for both categories of the device fabrication process followed and the device stress applications. The next chapter summarizes research findings and discusses potential follow-on work.

THIS PAGE INTENTIONALLY LEFT BLANK

V. CONCLUSIONS AND FUTURE WORK

A. CONCLUSIONS

This thesis had two objectives. The first was to streamline the sample preparation process to optimize and increase yield. The samples were successfully made utilizing the sample preparation procedure presented in Chapter III to maximize consistency, and yield while minimizing machine induced defects and dislocations due to I-beam exposure. We had zero sample breaks after optimizing the design.

Second, this thesis sought to chemically evaluate the areas near the gate edge and compare data for tends. We found that every device contained a dip and a foot area along the gate edge. A more severe dip and foot was observed in the Pt devices compared to Ni. All device samples stressed and unstressed lacked a GaN cap. A recommendation for future processing would be to grow a thicker GaN cap layer on top of the Nitronex, Inc© parts prior to processing. As the gate metal (Pt and Ni) diffused through the (Al, Ga)N layer but stopped diffusing at the GaN layer interface, a thicker GaN cap layer may reduce the diffusion rate within the gate.

Finally results showed there was a clear Si_3N_4 passivation layer present in all the samples examined. This layer did not change despite electrical stressing nor did it appear to diffuse into the (Al, Ga)N layer. However, there was oxygen present in all devices. Miao discussed in [21] the effect of oxidization in the 2DEG region. This was not the region we analyzed but his work does state that the unintentional presence of oxidation can have a variety of effects on the atomic and electronic structure of nitride surfaces.

B. FUTURE WORK

We established a clear sample preparation procedure and were able to extract the minimum sample set. NPS currently has a focused ion beam on campus and can now do most of the sample preparation. Our findings are based on a very small sample size. Additional work is needed on a larger sample set to compare these results and to verify our findings

In addition, we also were not able to quantify or weight the elements within the line scan process. Further thinning, high resolution TEM image, focal series reconstruction, and further electron dispersive spectrometry analysis is needed for this project.

Finally, this thesis compared electrically stressed devices to fresh samples. These devices would greatly benefit from other stress testing such as radiation stressing to investigate the potential reliability behavior of gallium nitride HEMTs.

APPENDIX MATLAB CODE

The Matlab code reads in the raw data from the Bruker detector and plots the data into Matlab. Once in Matlab, the date can be manipulated and concatenated to ensure the sample areas were analyzed in the same area for comparisons.

```
%Pt Line Scans
clear all
clc

%Pt Fresh Gate
load 'PtFreshGate.txt'
Distance=PtFreshGate(:,2)*1000;
Au=PtFreshGate(:,3);
Si=PtFreshGate(:,4)*0.1;
Al=PtFreshGate(:,5);
Ga=PtFreshGate(:,6);
N=PtFreshGate(:,7);
Pt=PtFreshGate(:,8);
O=PtFreshGate(:,9);

%Smooth the data
Au=smooth(Au);
Si=smooth(Si);
Al=smooth(Al);
Ga=smooth(Ga);
N=smooth(N);
Pt=smooth(Pt);
O=smooth(O);

figure (1)
plot(Distance,Au,Distance,Si,Distance,Al,Distance,Ga,Distance,N,Distance,Pt,Distance,
O)
grid on
title('Fresh Pt Gate Line Scan')
xlabel('Distance (nm)')
ylabel('Counts')
hleg1 = legend('Au','Si','Al','Ga','N','Pt','O');
set(hleg1,'Location','NorthEast')
set(0,'defaultAxesFontName', 'Times')

%Pt Fresh Foot
load 'PtFreshFoot.txt'
```

```
Distance=PtFreshFoot(:,2)*1000;
Au=PtFreshFoot(:,3);
Si=PtFreshFoot(:,4);
Al=PtFreshFoot(:,5);
Ga=PtFreshFoot(:,6);
N=PtFreshFoot(:,7);
Pt=PtFreshFoot(:,8);
O=PtFreshFoot(:,9);

%Smooth the data
Au=smooth(Au);
Si=smooth(Si);
Al=smooth(Al);
Ga=smooth(Ga);
N=smooth(N);
Pt=smooth(Pt);
O=smooth(O);

figure (2)
plot(Distance,Au,Distance,Si,Distance,Al,Distance,Ga,Distance,N,Distance,Pt,Distance,
O)
grid on
title('Fresh Pt Foot Line Scan')
xlabel('Distance (nm)')
ylabel('Counts')
hleg1 = legend('Au','Si','Al','Ga','N','Pt','O');
set(hleg1,'Location','NorthEast')
set(0,'defaultAxesFontName', 'Times')

%Pt Fresh Dip
load 'PtFreshDip.txt'
Distance=PtFreshDip(:,2)*1000;
Au=PtFreshDip(:,3);
Si=PtFreshDip(:,4);
Al=PtFreshDip(:,5);
Ga=PtFreshDip(:,6);
N=PtFreshDip(:,7);
Pt=PtFreshDip(:,8)*0.1;
O=PtFreshDip(:,9);

%Smooth the data
Au=smooth(Au);
Si=smooth(Si);
Al=smooth(Al);
Ga=smooth(Ga);
```

```
N=smooth(N);
Pt=smooth(Pt);
O=smooth(O);

figure (3)
plot(Distance,Au,Distance,Si,Distance,Al,Distance,Ga,Distance,N,Distance,Pt,Distance,
O)
grid on
title('Fresh Pt Dip Line Scan')
xlabel('Distance (nm)')
ylabel('Counts')
hleg1 = legend('Au','Si','Al','Ga','N','Pt','O');
set(hleg1,'Location','NorthEast')
set(0,'defaultAxesFontName', 'Times')

%Pt Fresh Active layer
load 'PtFreshActive.txt'
Distance=PtFreshActive(:,2)*1000;
Au=PtFreshActive(:,3)*0.1;
Si=PtFreshActive(:,4);
Al=PtFreshActive(:,5);
Ga=PtFreshActive(:,6);
N=PtFreshActive(:,7);
Pt=PtFreshActive(:,8)*0.1;
O=PtFreshActive(:,9);

%Smooth the data
Au=smooth(Au);
Si=smooth(Si);
Al=smooth(Al);
Ga=smooth(Ga);
N=smooth(N);
Pt=smooth(Pt);
O=smooth(O);

figure (4)
plot(Distance,Au,Distance,Si,Distance,Al,Distance,Ga,Distance,N,Distance,Pt,Distance,
O)
grid on
title('Fresh Pt Active Layer Line Scan')
xlabel('Distance (nm)')
ylabel('Counts')
hleg1 = legend('Au','Si','Al','Ga','N','Pt','O');
set(hleg1,'Location','NorthEast')
set(0,'defaultAxesFontName', 'Times')
```

THIS PAGE INTENTIONALLY LEFT BLANK

LIST OF REFERENCES

[1] M. A. Khan et al., "New developments in gallium nitride and the impact on power electronics," in *Power Electronics Specialists Conf.*, Recife, Brazil, 2005, pp. 15–26.

[2] E. L. Piner, "Integration of gallium nitride and silicon: from devices to diamond," in *IEEE International SOI Conf.*, Durango, CO., 2001, pp. 1–18.

[3] M. LaPedus, "Industry agrees on first 450-mm wafer standard," *Electrical Engineering Times*, October 22, 2008. Available: http://www.eetimes.com/document.asp?doc_id=1169573 [Accessed: March 1, 2014].

[4] W. Johnson and E.L. Piner, "GaN HEMT technology," *GaN and ZnO-based Materials and Devices*, Heidelberg: Springer–Verlag, 2012, pp. 209–237.

[5] J. D. Mones et al., "GaN HEMT reliability at 125°C for 1000 hours," in *IEEE Wide Bandgap Power Devices and Applications (WiPDA)Conf.*, Columbus, OH., 2013, pp. 174–177.

[6] C. G. Van de Walle, "Effects of impurities on the lattice parameters of GaN," *Physical Review B*, vol. 68, no. 16, 2003, pp. 209–214.

[7] P. Karmarrkar et al., "Proton irradiation effects on GaN-based high electron-mobility transistors with Si-doped $Al_xGa_{1-x}N$ and thick GaN cap layers," in *IEEE Transactions on Nuclear Science.*, vol. 51, no. 6, 2004, pp. 3801–3806.

[8] K. L. Holmes, "Two-dimensional modeling of aluminum nitride/gallium nitride high electron mobility transistor," M.S. thesis, Dept. of Elect. Eng., Naval Postgraduate School, 2002.

[9] K. P. Eimers, "2-D Modeling of GaN HEMTS Incorporating the Piezoelectric Effect," M.S. thesis, Dept. of Elect. Eng., Naval Postgraduate School, 2001.

[10] M. A. Porter, "Analysis of the piezoelectric effect at rf bias in gallium nitride high electron mobility transistors," M.S. thesis, Dept. of Elect. Eng., Naval Postgraduate School, 2011.

[11] Y. Wang, "Electrical and thermal analysis of gallium nitride HEMTs," M.S. thesis, Dept. of Appl. Phys., Naval Postgraduate School, 2009.

[12] S. D. Winchell, "Transport imaging in the one dimensional limit," M.S. thesis, Dept. of Appl. Phys., Naval Postgraduate School, 2006.

[13] D. A. Cary, “Ionizing radiation tolerance of a gallium nitride power transistor,” M.S. thesis, Dept. of Elect. Eng., Naval Postgraduate School, 2014.

[14] R. S. Pengelly et al, “A review of GaN on SiC high electron-mobility power transistors and MMICs,” in *IEEE Transactions on Microwave Theory and Technology*, vol. 60, no. 6, 2012, pp. 1764–1783.

[15] T. J. Anderson et al., “Reliability of GaN HEMTs: electrical and radiation-induced failure mechanisms,” in *Meeting of the Electrochemical Society Conf.*, San Francisco, CA, 2013, pp. 221–225.

[16] J. A. Del Alamo, “Nanometer-scale electronics with III-V compound semiconductors,” in *Nature*, vol. 479, 2011, pp. 317–323.

[17] R. Vetury, “The impact of surface states on the DC and RF characteristics of (Al, Ga)N /GaN HFETs,” in *IEEE Transactions on Electron Devices*, vol. 48, no. 3, 2001, pp. 560–566.

[18] J. Neugebauer and C. G. Van de Walle, “Gallium vacancies and the yellow luminescence in GaN,” in *Applied Physics Letters*, vol. 69, no. 4, 1996, pp. 503–505.

[19] P. D. Nellist, “Scanning transmission electron microscopy,” in *Science of Microscopy*, P. Hawkes, Ed. New York: Springer, 2007, pp. 65–70.

[20] L. K. Nan and L. M. Lung, “Study of FIB milling induced damage and contamination on ex-situ lift-out TEM specimen and methodology to reduce the artifacts,” in *IEEE International Symposium on the Physical and Failure Analysis of Integrated Circuits Conf.*, Suzhou, China, 2013, pp. 404–407.

[21] M. S. Miao et al., “Oxidation and the origin of the two-dimensional electron gas in (Al, Ga)N /GaN heterostructures,” in *Journal of Applied Physics*, vol. 107, no. 12, 2010, pp. 1–11.

INITIAL DISTRIBUTION LIST

1. Defense Technical Information Center
   Ft. Belvoir, Virginia

2. Dudley Knox Library
   Naval Postgraduate School
   Monterey, California